2016-01-01

A Geophysical Investigation At The Potrillo Maar

Manuel Moncada Gutierrez
University of Texas at El Paso, mmoncadagutierrez@miners.utep.edu

A GEOPHYSICAL INVESTIGATION AT THE POTRILLO MAAR

MANUEL MONCADA GUTIERREZ

Master's Program in Geophysics

APPROVED:

Diane I. Doser, Ph.D., Chair

Laura Serpa, Ph.D.

Terry Pavlis, Ph.D.

Oscar Dena, Ph.D.

Charles H Ambler, Ph. D.
Dean of the Graduate School

Dedication

I dedicate this thesis to my parents, Manuel Moncada and Olga Gutierrez, and my sisters, Janeth and America, and I thank them for their support.

A GEOPHYSICAL INVESTIGATION AT POTRILLO MAAR

by

MANUEL MONCADA GUTIERREZ

THESIS

Presented to the Faculty of the Graduate School of

The University of Texas at El Paso

in Partial Fulfillment

of the Requirements

for the Degree of

Master of Science

Department of Geological Sciences

THE UNIVERSITY OF TEXAS AT EL PASO

December 2016

Acknowledgment

First I want to thank my advisor Dr. Diane Doser for her patience and guidance for completing this thesis. Also, I want to thank the committee; Dr. Laura Serpa and Dr. Terry Pavlis, for they advise and suggestions during the academic and thesis process. I also want to thank Dr. Oscar Dena for his support in different ways to complete this research.

I want to thank the UTEP's staff: Dr. Phillip Goodell, Dr. Tina Carrick, Galen Kaip, Carlos Montana, Annette Veilleux and Joel Gilbert for the advice during the academic process.

I want to thank the people from the Universidad Autónoma de Ciudad Juárez (UACJ) for their support and helping with their resources to complete this thesis, Special thanks to Laura Molina, Jaqueline Ochoa, Oscar Ramirez, Azael Avalos, Miguel Galdean, Ernesto Duran, Martin Sandoval, Victor Avila, Carlos Castañeda and Michel Luna. I like to thank CONACYT for their support at the early stage of my MS degree.

Thanks to my colleagues for gave me their support. Thanks to Fellix Ziwu, Myra Guerrero, Jose Cervantes, Alex Sandoval, Marc Lucero, Juan Ochoa, Leslie Bernal, Alan Vennemann, Will Seelig, Richard Alfaro, Liza Castreñon, Luis Martinetti, Sandy Hardy, Arturo Ramirez and Yvette Pereyra.

Abstract

The Potrillo Volcanic Field (PVF) is a unique geological site located in Doña Ana County the southernmost part of New Mexico, and part of northern part of Chihuahua, Mexico. The main feature of the southern PVF is Potrillo Maar. This maar-volcano straddles the international boundary between United States and Mexico and lies within the southern part of the Rio Grande Rift. The Potrillo Maar was formed about 20,000 years ago in three major events that formed basalt lava flows and ejecta deposits that consist of crustal and mantle xenoliths.

The purpose of this thesis is to determine the area of the maar-diatreme, the severely fractured rock created by the explosion where the crater was made, and to estimate the thickness of its basalt layers using gravity, magnetics, and resistivity tomography surveys. These Potential field methods also provided a better understanding of the shallower structures of the near diatreme.

All the geophysical data was analyzed using the GM-SYS software package in order to create 2D cross section models to differentiate the diatreme, basalts and surrounding structures. Forward modeling has revealed a complex subsurface maar structure.

Modeling of 2-D cross-sections requires bodies with very low negative susceptibilities adequately match observations and error. These negative susceptibilities suggest that part of this diatreme composed of pre-maar volcanic that are older than the latest geomagnetic reversal. The diatreme has a depth of 125 m in the deepest part of the sections.

A basaltic feeder dike for the Potrillo maar was also imaged. The main dike is located in the center of the crater where three scoria cones are exposed at the surface. Other smaller dikes are located within the diatreme.

Table of contents

List of tables

List of figures

Chapter 1 Introduction

A maar-diatreme volcano is made by explosive eruptions that cut deeply into the country rock. A maar is defined as the crater surrounded by an ejecta ring, and as the diatreme structure continues downward it encloses the root zone deposits (White and Ross, 2011). Several geophysical studies such as gravity, magnetics and resistivity tomography, have been conducted at maar volcanoes around the world in order to investigate their subsurface structures. The Potrillo Maar, the focus of this thesis, straddles the international boundary between the United States and Mexico about 28 Km west of the El Paso-Juárez region and has so far not been geophysically studied. The study area is part of the Potrillo Volcanic Field, a series of volcanic features extending across southernmost Doña Ana County, New Mexico into northern Chihuahua, Mexico (Figure 1.1). The Potrillo Volcanic Field contains several other maars, including Killbourne Hole and Hunts Hole, which have been studied in more detail since they are easily accessible to researchers.

This study is comprised of two major objectives, the first being to assess the area of the diatreme, and the second to estimate the thickness of its basalt layers using gravity, magnetics, and resistivity tomography surveys. The resulting interpretations produced by this study add to the local and regional geologic understanding of the El Paso-Juarez area and Potrillo Volcanic Field. It will also add to the worldwide body of knowledge about the structures of maars.

The gravity survey was conducted using a Scintrex CG-5 gravimeter. Gravity data were collected at a total of 166 stations in the study area with 200 x 500 meter grid spacing to obtain the Residual Bouguer Anomaly as the final product after corrections. Magnetics were carried out using a GEM systems, GSM-19 Overhauser magnetometer as the rover, and the Geometrics G-857 magnetometer as a base station. Readings were recorded every 200 meters in N-S direction and every 500 meters in an E-W direction. The daily magnetic field variation was subtracted from the

data and then the data were processed to obtain the Reduced To Pole (RTP) magnetic field. A tomographic resistivity survey was carried out with a Terrameter SAS4000 system composed of 4 cables, each 200m in length with a10m spacing between electrodes along the cable.

The data collected in my field work was modeled using GM-SYS software to obtain two dimensional geophysical cross sections. These models define the igneous rocks, the diatreme, surrounding structures and the thickness of the basalt layer. When combined with surface mapping the structures provide insights into the geometry of the maar and are compared to structures of other maars around the world.

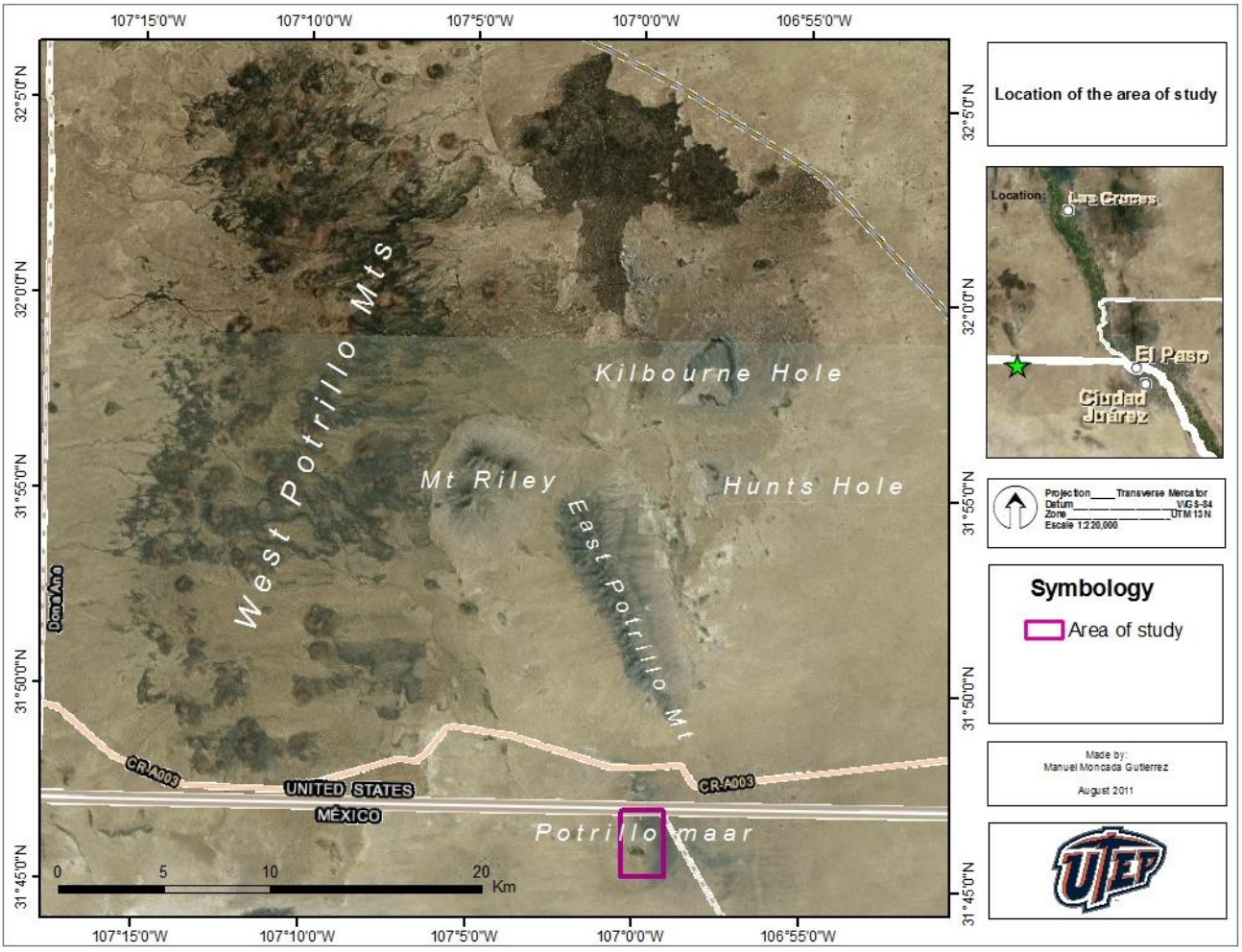

Figure 1.1 This map shows the location of the area of study.

Chapter 2 Geology of the area

The Potrillo Maar lies within the southern part of the Rio Grande Rift, (Figure 2.1) where the continental crust is thought to have formed during the Mazatzal orogeny between ~1.7-1.6 Ga. (e.g. Karlstrom et al., 2004). The Mazatzal orogeny was accreted to Laurentia around 1.65-1.60 Ga. From 1.60 to 1.50 Ga the lithosphere of southwestern Laurentia was stable as there is no evidence of magmatism and tectonism of this age. From 1.48-1.35 Ga was a period marked by variable deformation and metamorphism due to an intracratonic tectonic event that reactivated the older structures. This was followed by constant tectonism in southern New Mexico and western Texas from 1.48 to 1.08 Ga suggesting a convergent margin at the southern boundary of Laurentia, and concluding with the Grenville orogeny which is characterized by A-Type magmatism believed to have formed in an extensional or transtensional environment (Shannon et al., 1997; Bickford et al., 2000).

The Potrillo maar also lies on the eastern edge of the Laramide orogeny that occurred approximately 75-43 Ma (Chapin and Cather, 1981), when this area experienced major crustal shortening (Seager and Mack, 1985). This contractional episode broke the crust of southwestern New Mexico into a series of basement-cored uplifts and yoked basins (Seager, 2004). Laramide deformation apparently culminated in the Paleocene and Eocene and it was follow by extension associated with the Rio Grande Rift beginning at ~35 Ma (McMillan et al., 2000). Plutonism in the Rio Grande Rift occurred at 27-26 Ma, according to the estimated ages of igneous xenoliths from the Potrillo Volcanic Field (PVF) that are believed to be part of a large plutonic complex in the mid-crust (Li et al., 2004). The southern Rio Grande Rift is characterized by extensional block faulting and basin subsidence and is associated with eruptions of silicic calderas and lithosphere derived mafic lava flows (Mack, 2002). According to Williams (1999), the PVF formed between

900,000 and 40,000 years ago, and within this field three maar volcanoes formed: Kilbourne Hole (30,000 ± 15,000 ya), Hunt's Hole (17,000 ± 7,000) and Potrillo maar (59,000 ± 6,000 ya) (Hoffer, 2001).

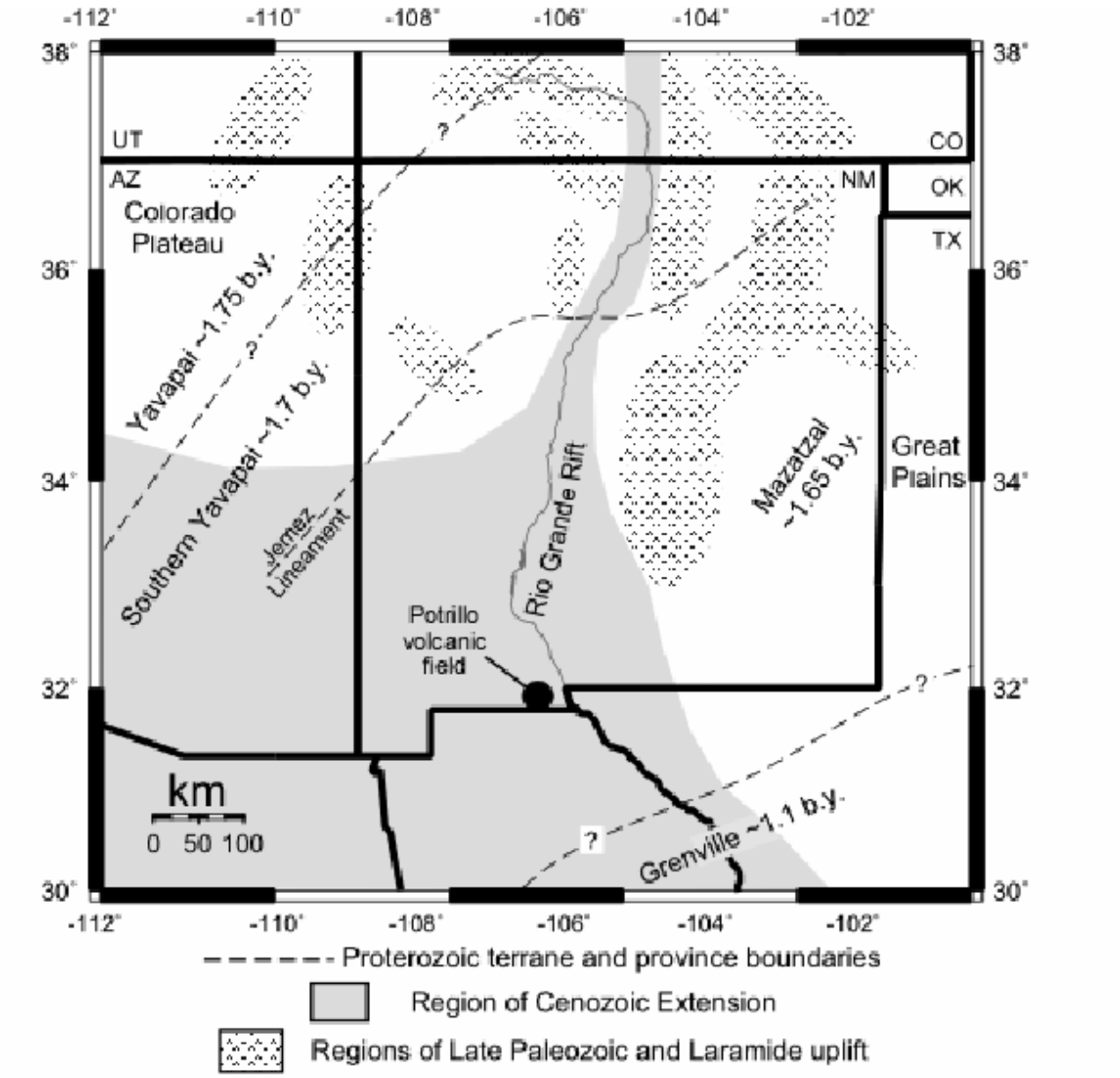

Figure 2.1 Map of the Rio Grande Rift region showing Proterozoic terrane boundaries, regions of with Laramide uplift, and regions of Cenozoic extension. Modified from Hamblock (2006).

Potrillo Maar stratigraphy

The Camp Rice Formation is the oldest unit exposed at the Potrillo Maar (Strain, 1996). The Camp Rice Formation of approximately Pliocene age, represents fluvial facies characterized by a moderately well-bedded, well-developed, concretionary caliche conglomerate containing lenses of friable sandstones (Hoffer 2001). Pre-maar volcanism has been identified at the northern end of the maar with a 1-2 m thick basalt lava flow lying on top of the Camp Rice formation. Above this basalt layer a 10-12 m high cinder cone has been identified. The lava associated with the cinder cone is vesicular and contains abundant mantle xenoliths. The ejecta deposits exposed at Potrillo Maar consist of base-surge deposits, airfall materials, crustal and mantle xenoliths (Hoffer 2001). Three major units have been interpreted from these deposits (Waggoner 1990). The upper deposits form cliffs from large basaltic blocks and bombs and mantle and crustal xenoliths. The middle unit is greater in extent and forms gentle slopes, in contrast to the upper unit. The lower unit forms a basalt cliff and exhibits cross-bedding and accretionary lapilli. The post maar volcanism is related to 3 major cinder cones and 6 small spatter cones located at the southern end of the Potrillo Maar. The youngest units in the Potrillo Maar are recent playa deposits and eolian sand. These deposits are found on the west, northeast and south sides of the post maar basalt flows. The playa deposit consists of silt to clay-sized particles (Figure 2.2).

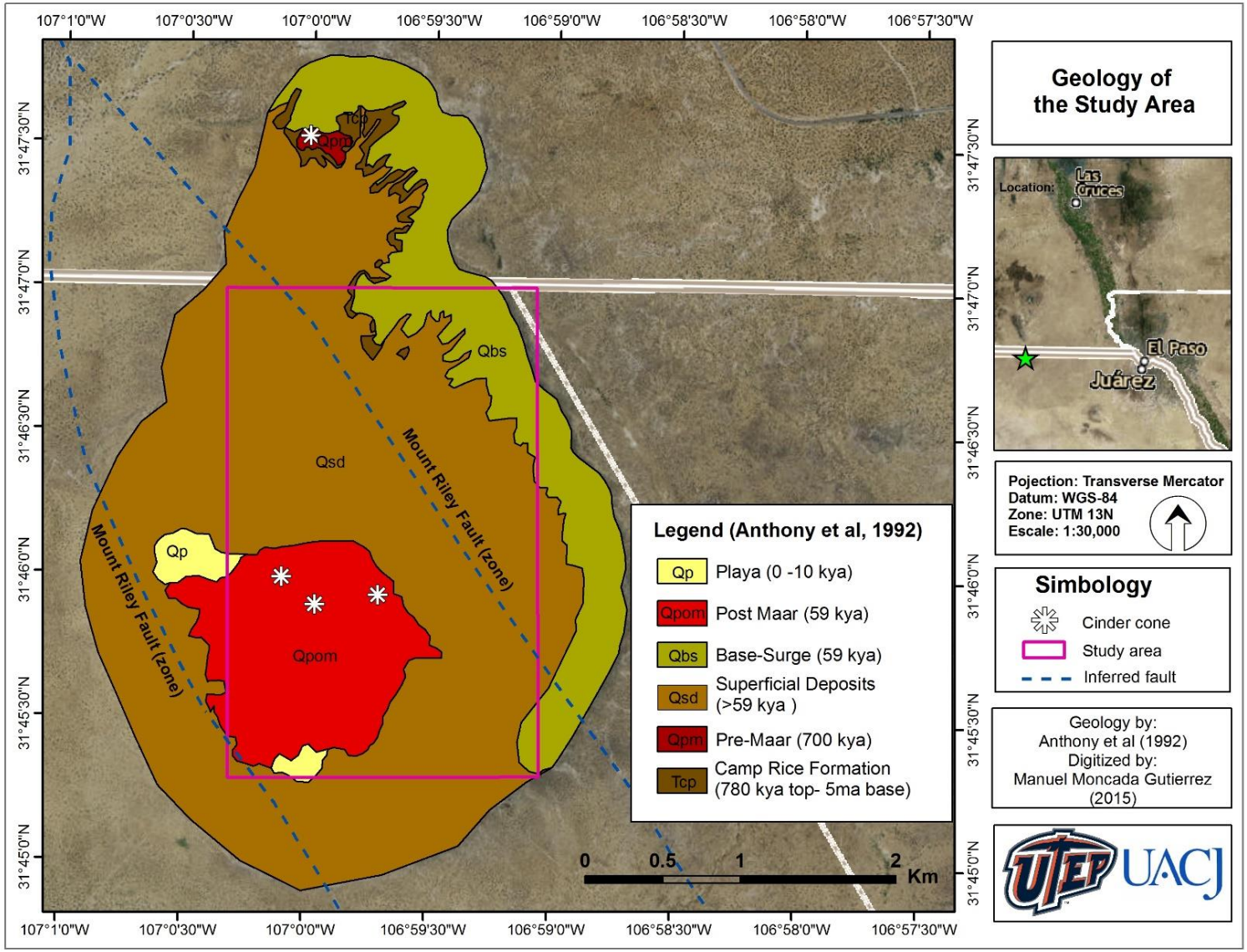

Figure 2.2 Geology of the area of study (modified from Anthony et al, 1992).

Chapter 3 Previous studies

Several Geophysical studies have been conducted at maar volcanoes around the world in order to investigate their subsurface structures. Skácelová et al (2010, Figure 3.1) studied partly eroded maar-diatreme volcanoes in the northern part of the Czech Republic. One of the maar volcanoes is the Hnojnice Diatreme that forms part of the České Středohoří Volcanic Complex (CSVC) with an age ranging from the Oligocene (33.9 to 23 ma) to the late Miocene (11.6 to 5.3 ma). The second volcano is the Rychnov Maar that is part of the Bohemian Massif which ranges in age from the Late Cretaceous (100.5 to 66 ma) to Oligocene. This maar is situated within crystalline rocks.

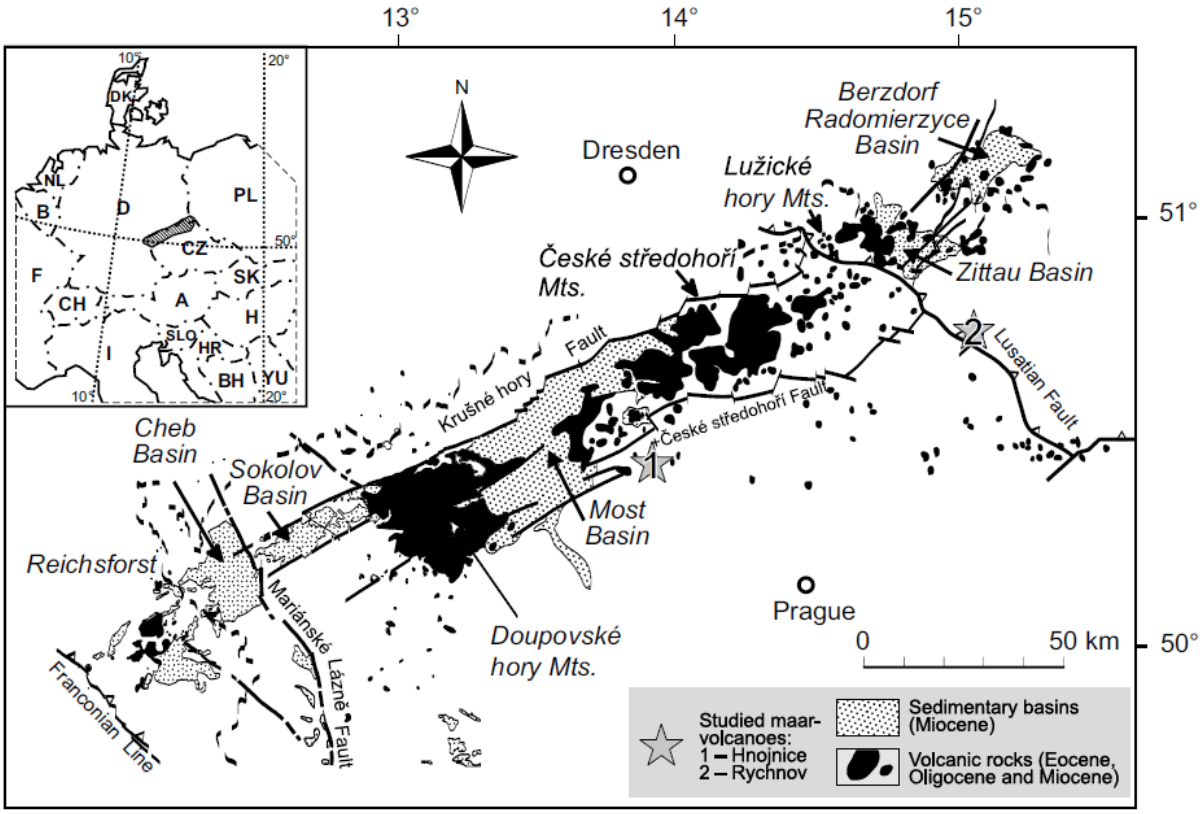

Figure 3.1 Location of the maar volcanoes studied in the Czech Republic by Skácelová et al (2010).

The second study was performed by Cassidy et al (2006) in the Pukaki, Pukekiwiriki, Domain and Waitomokai Maars located in the Auckland volcanic field, New Zealand (Figure 3.2). These maars have circular raised tuff rings and slightly depressed craters that are filled with recent sediments. The maar volcanoes are hosted by Plio- Pleistocene sediments (5 ma to 12 kya), except the Domain Volcano, which is hosted by Miocene sedimentary rock.

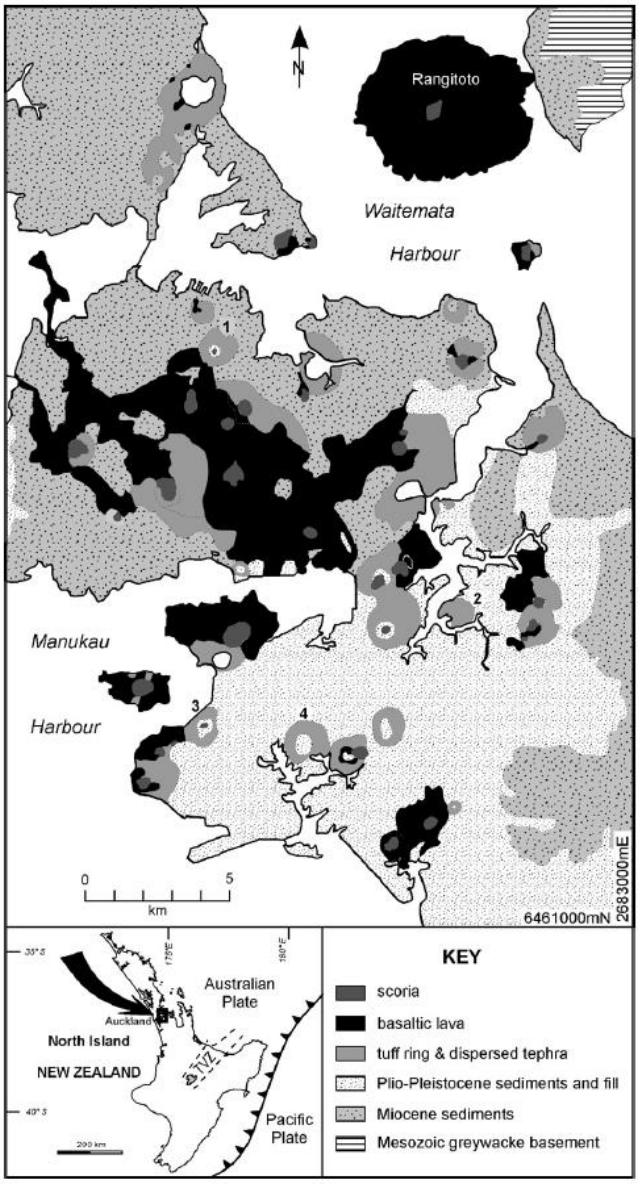

Figure 3.2 Location of the maar volcanoes in New Zealand: 1) Domain 2) Pukekiwiriki 3) Watomokai 4) Pukaki.

The third study was performed by Maksim (2016) in Killbourne Hole, a phreatomagmatic crater that forms part of the northern Potrillo Volcanic Field (Figure 3.3). This crater has is 2 km wide and is 200 m deep (Reiche, 1940). Seager (1987) estimated that the eruption occurred 0.02-0.01 Ma. This explosion deposited 50 to 150 m of pyroclastic deposits (Hoffer, 1971; Hawley 1975). After this, aeolian and fluvial material were deposited in the crater, covering the structures and diatreme in it.

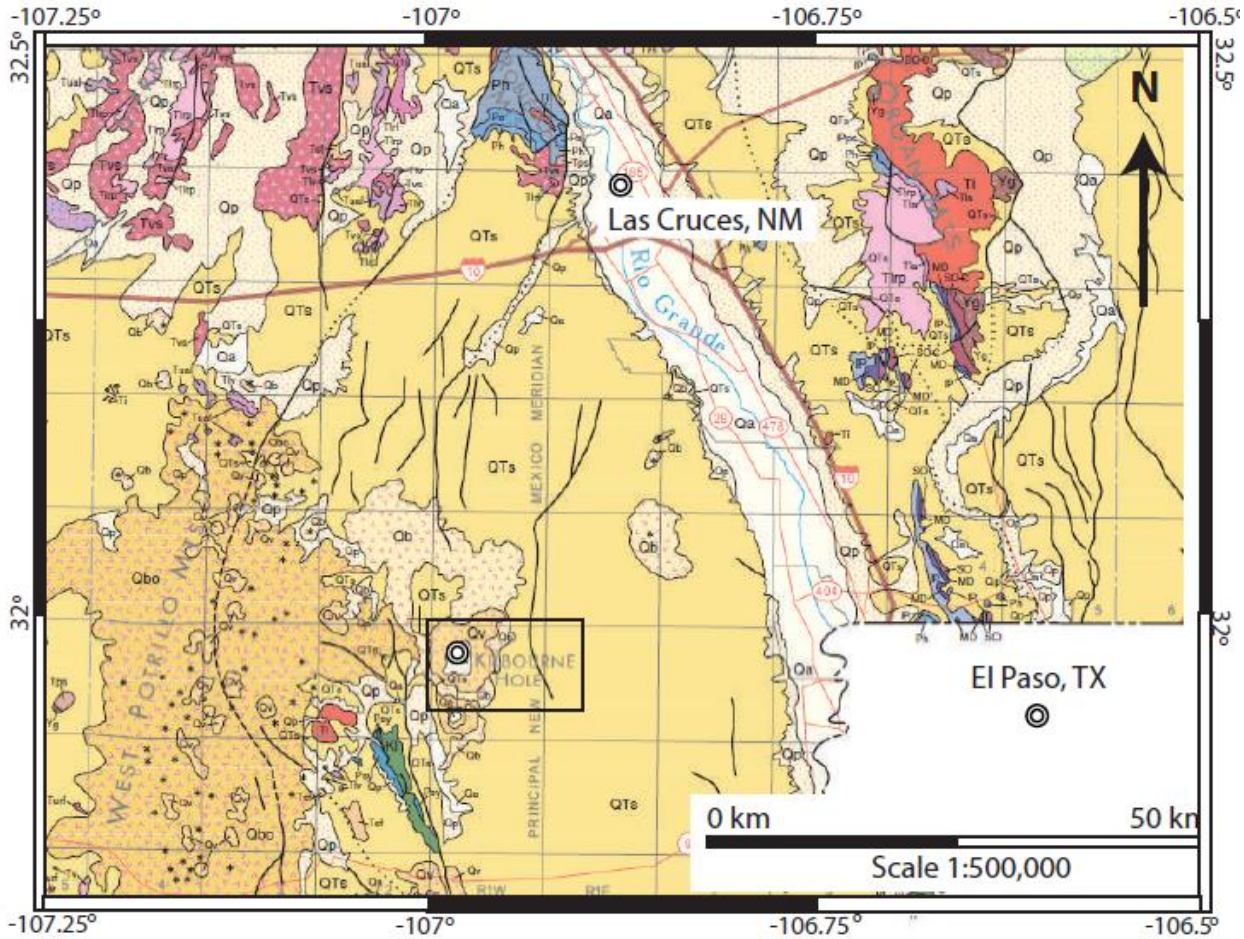

Figure 3.3 Map that shows the geology and location of Killbourne Hole in Doña Ana County, New Mexico.

Gravity and magnetic surveys had been conducted in these studies of maars, but only the research by Skácelová et al (2010) used the tomographic resistivity technique. The gravity and magnetic methods give very good estimates of the basalt and diatreme thicknesses. When the data are used jointly, they were also able to locate dikes that act as the feeders for some of the maars (e.g.Hnojnice Diatreme, Hole) (Figure 3.4 and 3.5). The resistivity data gave a well resolved image of the shallow subsurface structures (Figure 3.6), and also resolved the difference between the weathered and the unweathered rocks, however, the depth penetration of this method depends on the length of the electrode arrangement.

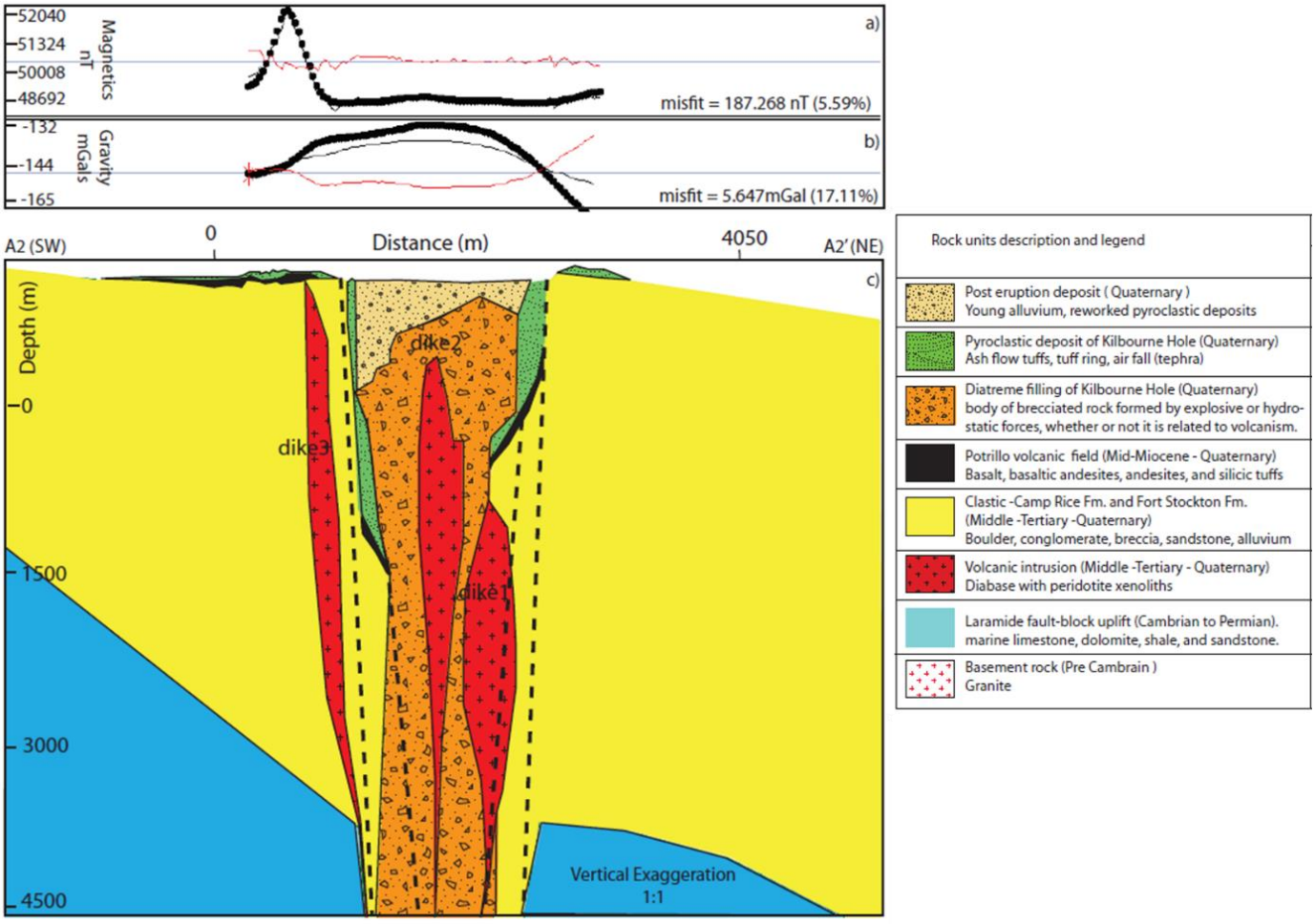

Figure 3.4Profile made by Maksim (2016) at Killbourne Hole, showing the structures obtained from the inversion of gravity and magnetic data.

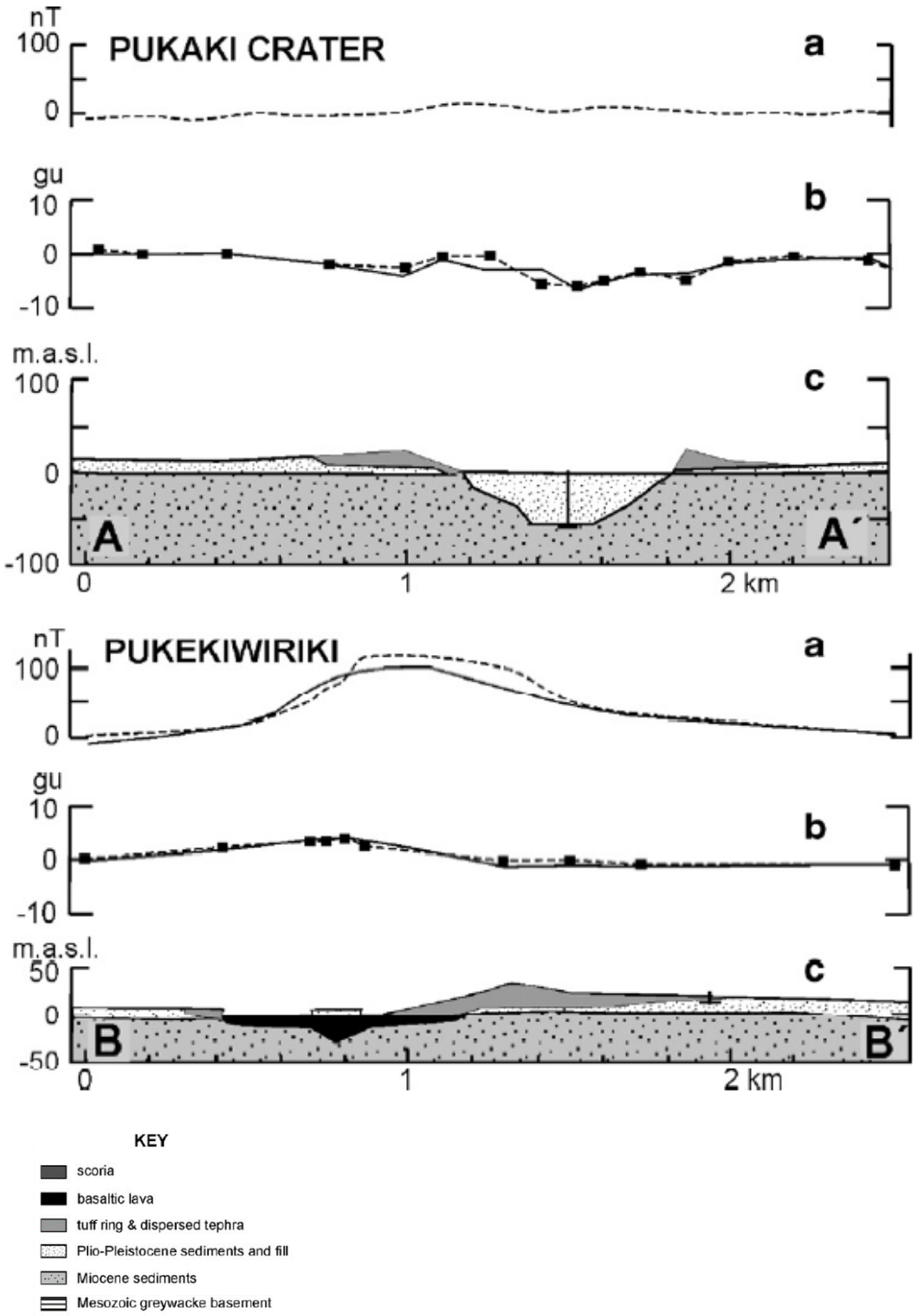

Figure 3.5 Cross sections from the Pukaki and Pukekiwiriki volcanoes that show the magnetic and gravity responses (a and b) where the observed responses are the dashed lines and the calculated are the solid lines. (Cassidy et al, 2006).

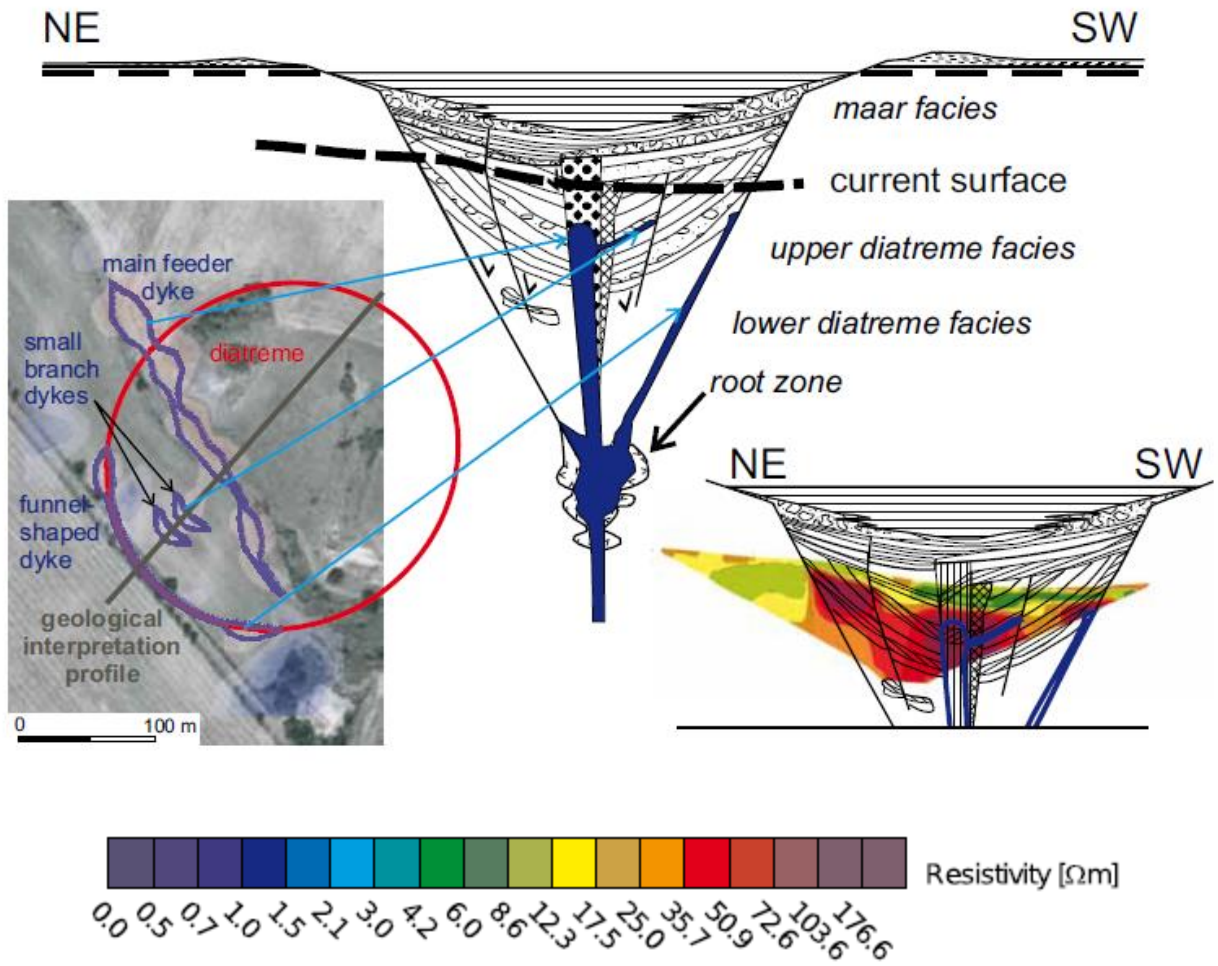

Figure 3.6 Interpretation of the resistivity tomography study by Skácelová et al (2010). Low resistivities are attributed to the diatreme (Cretaceous marlstones, claystones and Quaternary fluvial deposits). Resistivity values around 20 ohm-m and 50 ohm-m are interpreted as basalt dikes and diatreme breccias. The highest resistivities (> 50 ohm-m) are cause by the coherent basaltic body that acts as the main feeder of the maar volcano.

Chapter 4 Methodology

Data collection

Potential field methods (gravity and magnetic surveys) combined with a multi-electrode resistivity survey were used to map the area of study using equipment owned by Universidad Autónoma de Ciudad Juárez (UACJ). The gravimetric survey was conducted using a Scintrex CG -5 gravity meter with a standard resolution of 1 microGals and noise reduction system. A total of 166 gravity stations were collected in the study area with 200 meter spacing in a north-south direction and 500 meter spacing in an east-west direction, inside the crater. A 200 meter spacing was used between points on dirt roads surrounding the crater and one reading was made on top of each basalt cone (Figure 4.1). Each data point was required to meet the following quality standards:

- Two readings per station (30 measurements averaged for each reading) with less than a 0.003 mGals of difference between them.
- Tilt (gravimeter level) needed to be ± 4 Arctg or less.
- Less than 0.040 mGals in the standard deviation between readings.
- Less than 3 rejections per reading (measurements rejected due to random noise).

Elevation control was obtained from a GPS Sokkia GRX1 using static points of 5 minutes duration at each of the points. This equipment can receive multiple signal types (GPS, GLONASS, etc) and when combined, gives a very accurate horizontal and vertical estimation of position (3mm and 10mm, respectively).

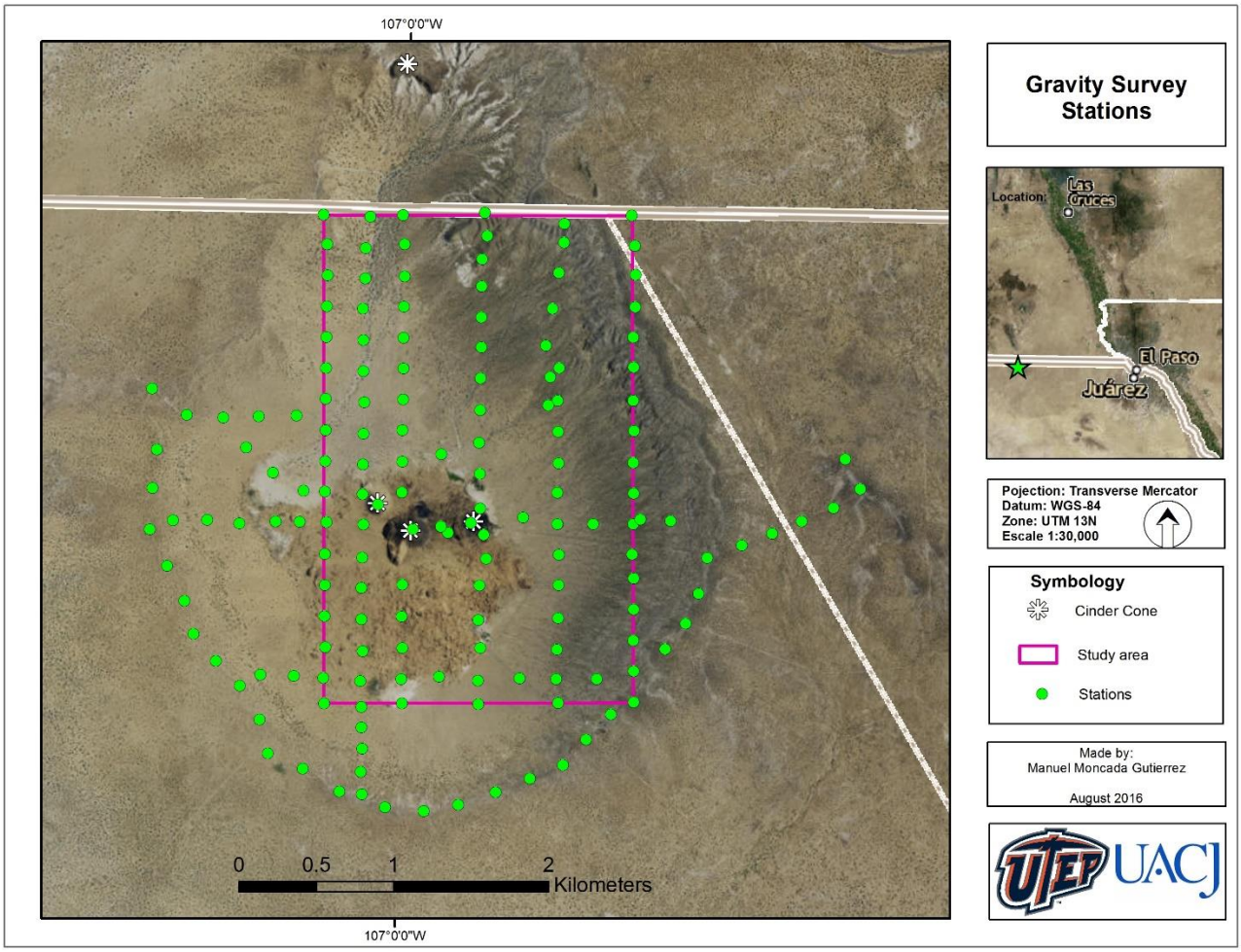

Figure 4.1 Map showing gravity measurements (green points) in the study area (purple box) within Potrillo Maar.

Magnetic field measurements were carried out using the GEM Systems GSM-19 Overhauser Magnetometer as the rover and UTEP's Geometrics G-857 magnetometer as the base station. A total of 240 magnetic readings were taken approximately every 200 meters in the north-south direction and every 250 meters in the east-west direction in the crater, with a 200 meter spacing between points on dirt roads, and about 3 points were taken on top of the each basalt cone (Figure 4.2).

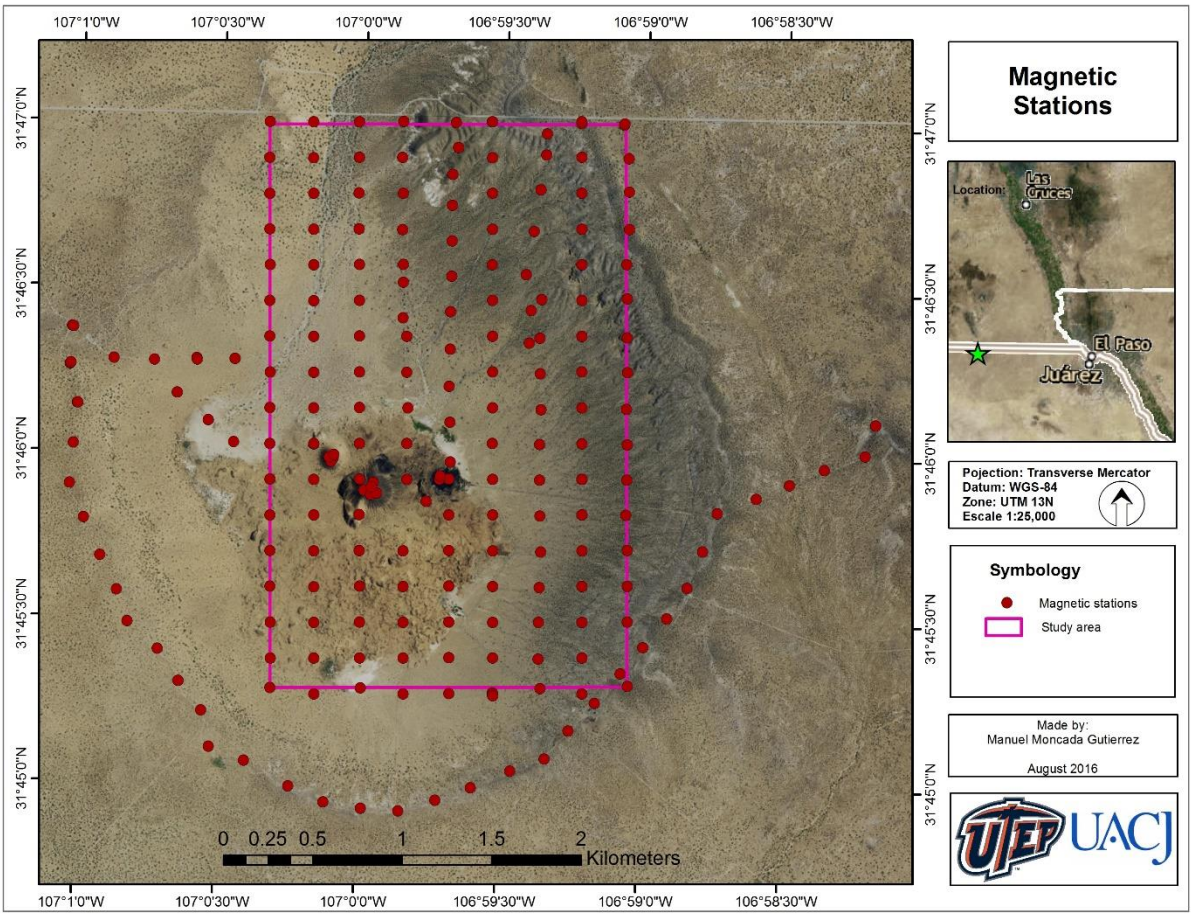

Figure 4.2 Map showing magnetic measurements (green points) in the study area (purple box) within Potrillo Maar.

Tomographic resistivity surveys were carried out with a Terrameter SAS4000 using 4 cables each 200 m in length with 10 m spacing between electrodes along each cable. The pole-dipole arrangement (Figure 4.3) was preferred because has a depth of penetration of about 200 meters.

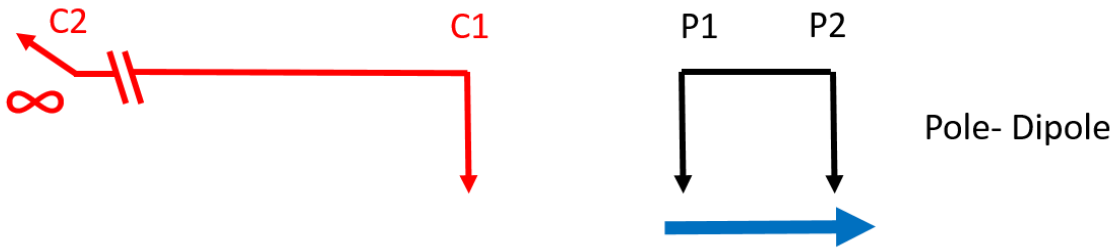

Figure 4.3 Arrangement configuration of the electrodes for a pole-dipole resistivity survey. “C” denotes current electrode and “P” potential electrode.

The tomography lines were originally planned to cross the cinder cones, however, these lines were moved based on the anomalies observed by the combination of the gravity and magnetic surveys (Figure 4.4).

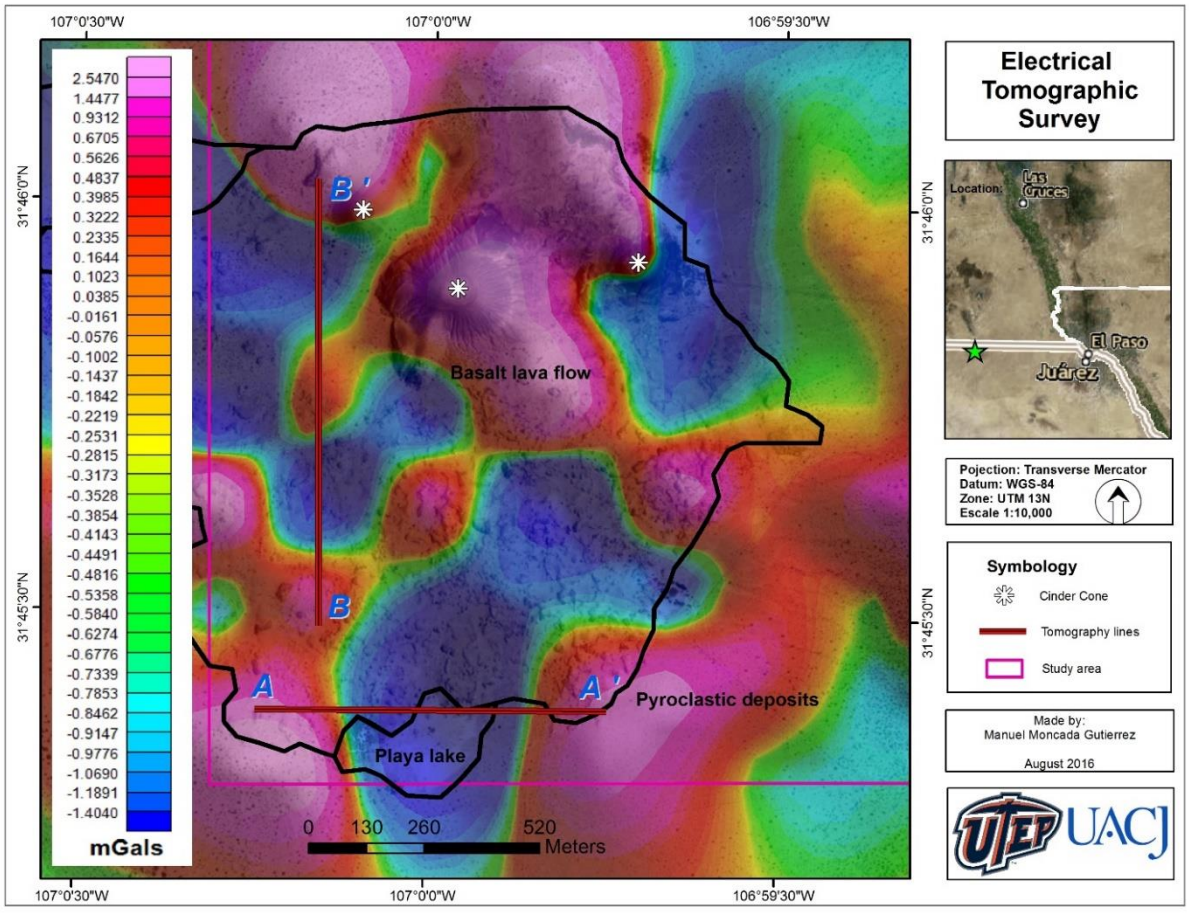

Figure 4.4 This map shows the location of the electrical resistivity tomographic surveys (red lines) in the area of study.

Data processing - Gravity

Gravity readings that did not meet the quality standards outlined previously were removed. After this step, corrections for drift/tides, latitude and free air were applied. Following this, simple Bouguer corrections were obtained with a reduction density of 2.67 g/cc.

Terrain corrections were applied by using local and regional topographic models taken from the static GPS points and a Digital Elevation Model (DEM) from the Servicio Geológico Mexicano (SGM), respectively. This information is required to obtain the Complete Bouguer Anomaly (CBA) given by:

$$\Delta g_{CBA} = g_{OBS} - g_{FA} - g_{SB} - g_{TC} - g_0$$

Where g_{OBS} is the observed gravity, g_{FA} is the free air anomaly, g_{SB} is the simple Bouguer anomaly, g_{TC} is the terrain correction and g_0 is the observed. Next I obtained the Residual Bouguer Anomaly (RBA) by the subtraction of the contributions of regional anomalies from the Complete Bouguer Anomaly (CBA) by fitting a third-order polynomial to the longer wavelength regional trends (Figure 4.5). This process enhances gravity anomalies due to shorter wavelength, local features.

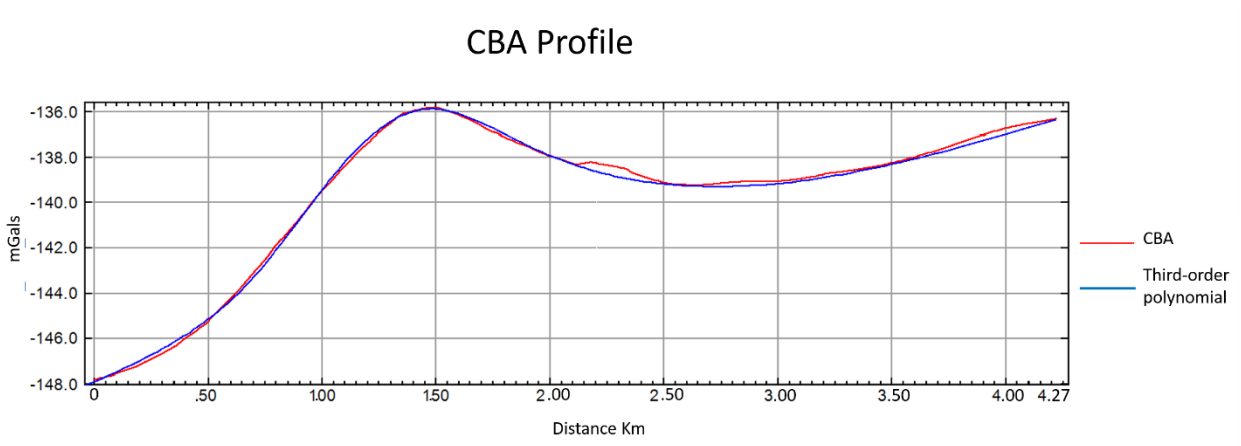

Figure 4.5 A profile from the CBA (red line) compared to the third order polynomial (blue line). This third order trend is removed from the CBA to obtain the Residual Bouguer Anomaly reflecting local variations in gravity.

This is done by applying an upward continuation filter to obtain the long wavelength signals (regional gravity). Then, this long wavelength signal is removed from the CBA to obtain the RBA. All of these corrections were applied with Geosoft's Oasis Montaj software package.

Data processing – magnetics

Data from the two magnetometers was formatted differently; the data needed to be converted to the same format before applying the diurnal correction (Figure 4.6). This correction accounts for the daily variations (drift) of the magnetic field observed at the base station. A datum of 47500 nT was used for the area and corrections were obtained from:

$$B\text{corrected} = B\text{rover} - Bbase + Datum$$

The program GEMLink from GEM systems, was used to compute the correction.

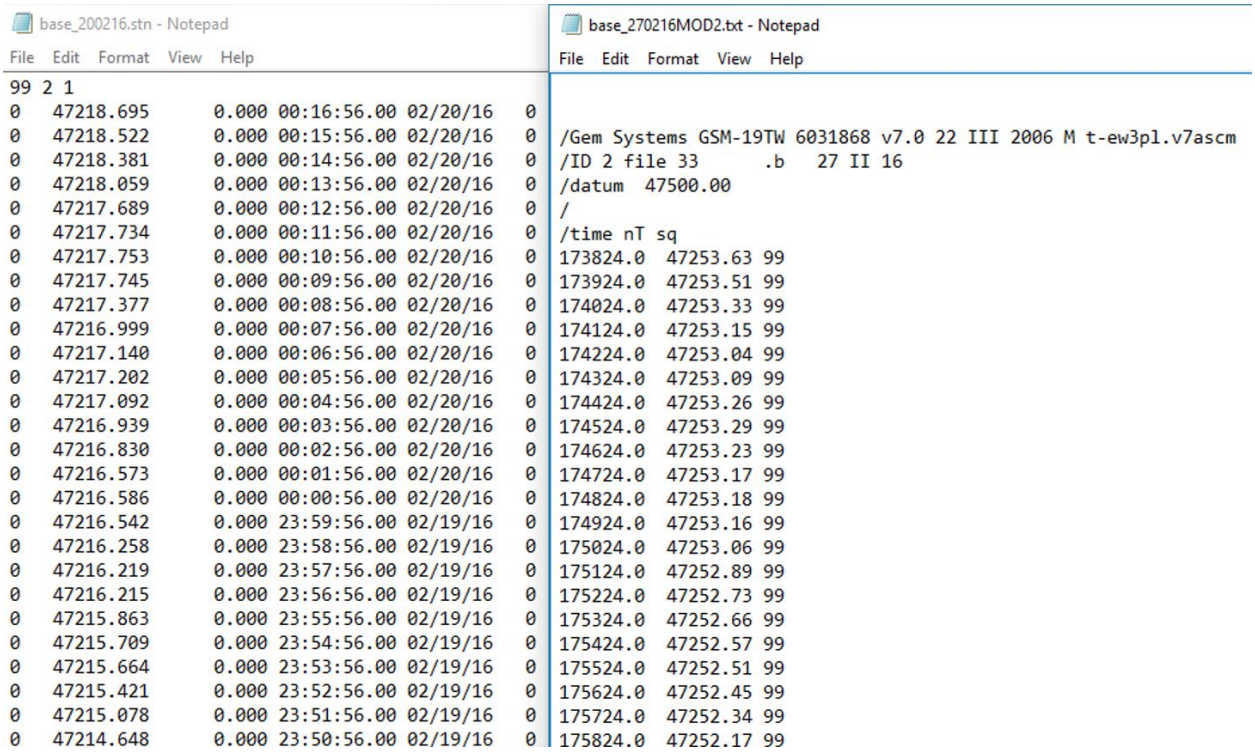

base_200216.stn - Notepad

File Edit Format View Help

```
99 2 1
0   47218.695      0.000 00:16:56.00 02/20/16   0
0   47218.522      0.000 00:15:56.00 02/20/16   0
0   47218.381      0.000 00:14:56.00 02/20/16   0
0   47218.059      0.000 00:13:56.00 02/20/16   0
0   47217.689      0.000 00:12:56.00 02/20/16   0
0   47217.734      0.000 00:11:56.00 02/20/16   0
0   47217.753      0.000 00:10:56.00 02/20/16   0
0   47217.745      0.000 00:09:56.00 02/20/16   0
0   47217.377      0.000 00:08:56.00 02/20/16   0
0   47216.999      0.000 00:07:56.00 02/20/16   0
0   47217.140      0.000 00:06:56.00 02/20/16   0
0   47217.202      0.000 00:05:56.00 02/20/16   0
0   47217.092      0.000 00:04:56.00 02/20/16   0
0   47216.939      0.000 00:03:56.00 02/20/16   0
0   47216.830      0.000 00:02:56.00 02/20/16   0
0   47216.573      0.000 00:01:56.00 02/20/16   0
0   47216.586      0.000 00:00:56.00 02/20/16   0
0   47216.542      0.000 23:59:56.00 02/19/16   0
0   47216.258      0.000 23:58:56.00 02/19/16   0
0   47216.219      0.000 23:57:56.00 02/19/16   0
0   47216.215      0.000 23:56:56.00 02/19/16   0
0   47215.863      0.000 23:55:56.00 02/19/16   0
0   47215.709      0.000 23:54:56.00 02/19/16   0
0   47215.664      0.000 23:53:56.00 02/19/16   0
0   47215.421      0.000 23:52:56.00 02/19/16   0
0   47215.078      0.000 23:51:56.00 02/19/16   0
0   47214.648      0.000 23:50:56.00 02/19/16   0
```

base_270216MOD2.txt - Notepad

File Edit Format View Help

```
/Gem Systems GSM-19TW 6031868 v7.0 22 III 2006 M t-ew3p1.v7ascm
/ID 2 file 33      .b   27 II 16
/datum  47500.00
/
/time nT sq
173824.0  47253.63 99
173924.0  47253.51 99
174024.0  47253.33 99
174124.0  47253.15 99
174224.0  47253.04 99
174324.0  47253.09 99
174424.0  47253.26 99
174524.0  47253.29 99
174624.0  47253.23 99
174724.0  47253.17 99
174824.0  47253.18 99
174924.0  47253.16 99
175024.0  47253.06 99
175124.0  47252.89 99
175224.0  47252.73 99
175324.0  47252.66 99
175424.0  47252.57 99
175524.0  47252.51 99
175624.0  47252.45 99
175724.0  47252.34 99
175824.0  47252.17 99
```

Figure 4.6 This image shows two different formats used by the instruments. On the left is the format from the Geometrics G-857 magnetometer showing magnetic intensity (column 1), time (column 2) and date (column 3). On the right is the format from GEM Systems GSM-19 Overhauser Magnetometer showing time (column 1) and magnetic intensity (column 2).

The Reduce To Pole (RTP) filter is an important filter that needs to be applied to the magnetic field data. The data is influenced by the effects of the inclination and declination of the geomagnetic field, these offsets cause of the observed anomalies from true locations of the causative bodies, where the RTP eliminates these effects. In practical terms it models the anomalies as if they were measured at the magnetic pole (vertical magnetic inclination). High magnetic values are focused directly on the source that produces them and the gradient reaches a maximum value at the boundary of the anomalous body (Figure 4.7).

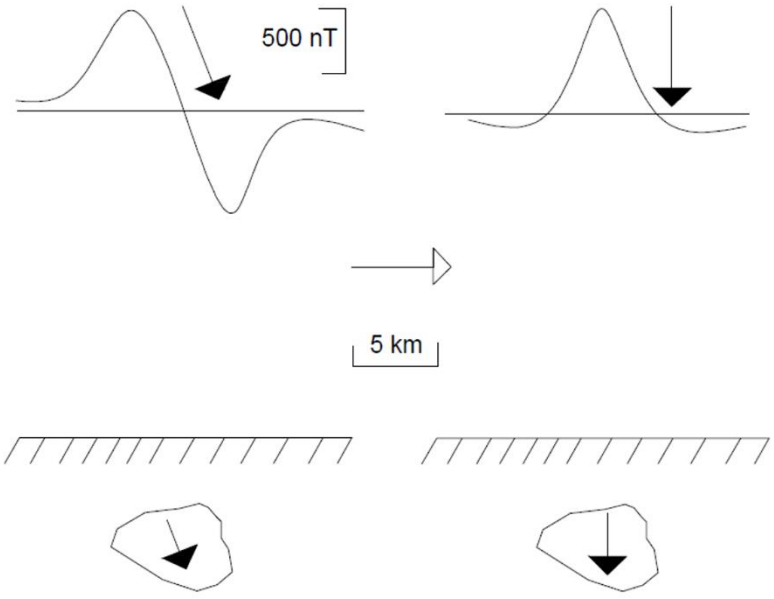

Figure 4.7 It ilustrates the direction of a signal from a source in the magnetic field at the study area latitude (left) versus the signal of the source after the RTP filter is applied to it.

Data processing – electrical tomographic survey

Data were processed and inverted using the program RES2DINV after bad data points were eliminated (Figure 4.8). Following this step, elevation was assigned to each of the electrodes. This was needed for correctly invert for structural depths.

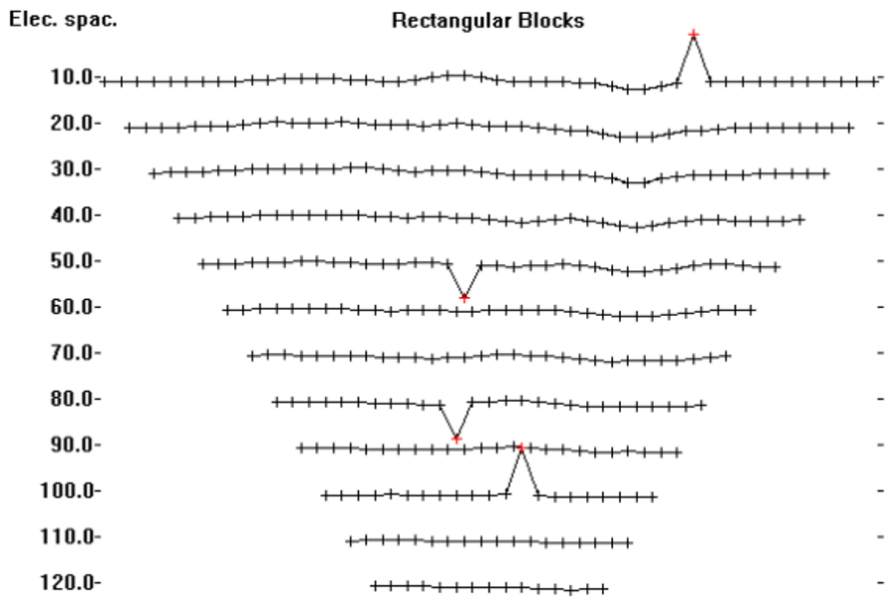

Figure 4.8 An example of a resistivity data set with some bad points (red crosses). Bad points are removed from the actual data to help minimize the error at the end of the inversion (RES2DINV manual, 2010).

The inversion method used by the program is the smoothness-constrained least squares method (deGroot-Hedlin and Constable, 1990; Sasaki, 1992; RES2DINV manual, 2010,) where:

$$(J^T J + uF)d = J^T g$$

Where:

$F = f_x f_x^T + f_z f_z^T$

$f_x = horizontal\ flatness\ filter$

$f_z = vertical\ flatness\ filter$

$J = matrix\ of\ partial\ derivatives$

$u = damping\ factor$

$d = model\ pertubation\ vector$

$g = discrepancy\ vector$

The goal of this inversion is to obtain the best possible model with lowest RMS error and consistent with known geology.

2D data modeling

Using models from previous geological and geophysical studies of maars (e.g. Maksim 2016, Skácelová 2010) I built two dimensional models as starting point for matching the observed gravity and magnetics data with the calculated data. The GM-SYS software is based on Talwani et al (1959) and Talwani and Talwani and Heirtzler (1964).

Chapter 5 Data analysis

Gravity maps

A provisional (CBA) gravity map was made by merging data collected by UACJ (Universidad Autónoma de Ciudad Juárez) with the UTEP (University of Texas at El Paso) (Figure 5.1). As expected, the highest values in gravity anomalies are associated with the PVF and mountain ranges (Franklin Mountains, Sierra de Juarez). Between the PVF and the mountain ranges are lower gravity anomaly values related to the Mesilla Bolson. Moreover, lower anomaly values located on the east side of the map are related to the Hueco Bolson.

The CBA map of the local study area reflects the main geologic features surrounding the study area (Figure 5.2). High gravity anomaly values are related to the main feeder of the maar volcano and extend to the south until they end at the edge of the basalt flows at the surface. Similarly, the high anomaly values extend to the north and northeast part of the map where they appear to spread to the U.S. part of the maar where the pre-maar cone is located. Lower anomaly values are situated in the most southernmost part of the map. These values are associated with sediments and the tephra ring caused by the explosion. By superimposing the CBA map from the local Potrillo Maar study area on the CBA map (Figure 5.3), it is apparent that the local highs merge with the regional highs of the PVF.

The RBA map (Figure 5.4) shows shallower gravity anomalies that are similar to the CBA map, where high gravity anomaly values are related to the main feeder dike located at the center of the map but are more influenced by the basalt flows at the surface. High gravity anomalies in the northern part of the RBA are lower than in the CBA map. This means that the principal feature that controls the gravity anomaly high is deeper. This high signature may be associated with the pre-maar ejecta deposits. The lower gravity anomaly values that surround the main feature of the

maar volcano are related to the tephra ring that is principally composed of sand, silt and tuff (Reeves and De Hon 1965).

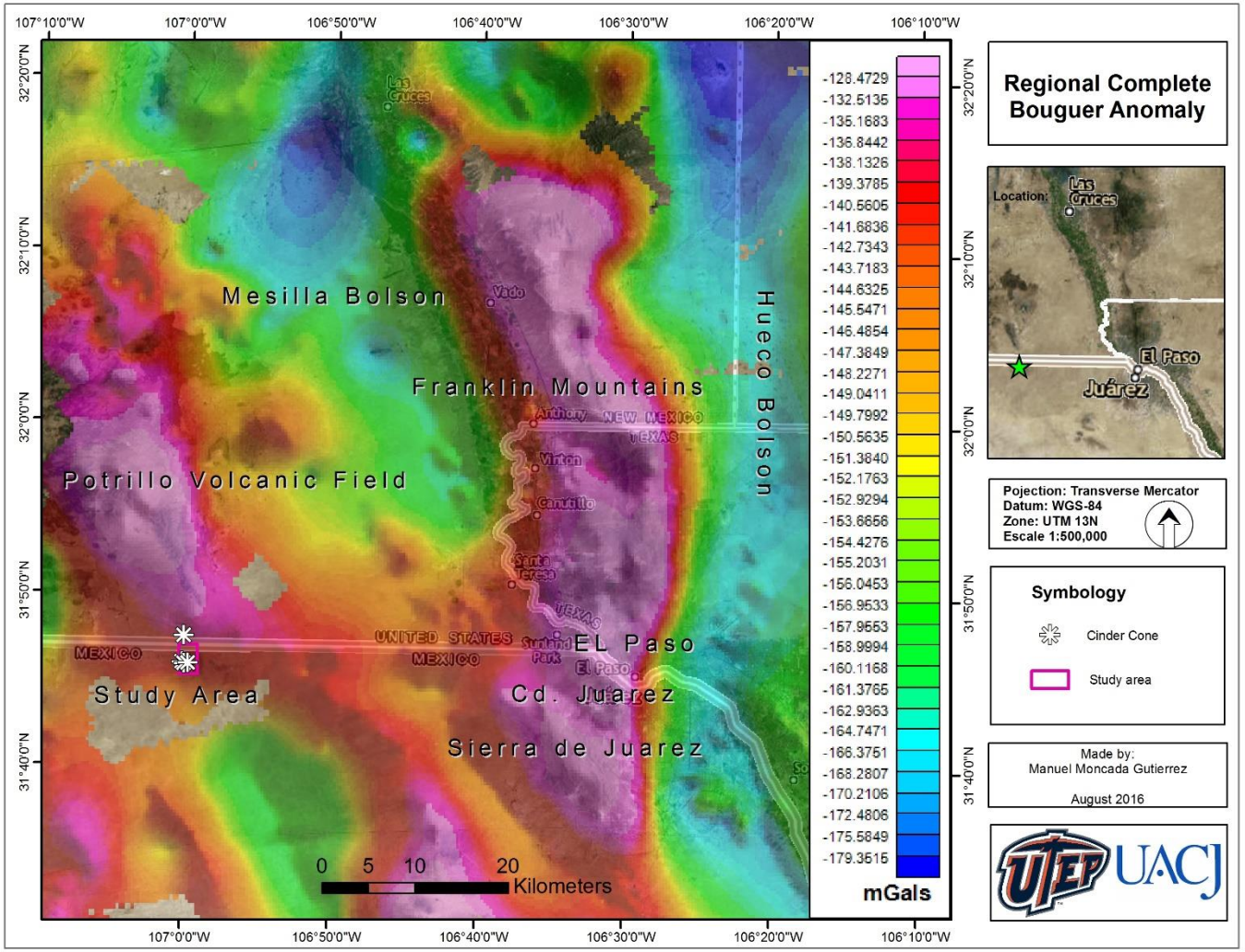

Figure 5.1 The Complete Bouguer anomaly values for the El Paso- Juarez region. High values are related to mountain ranges (yellow to pink colors) and low values are related to the basins (blue to green colors).

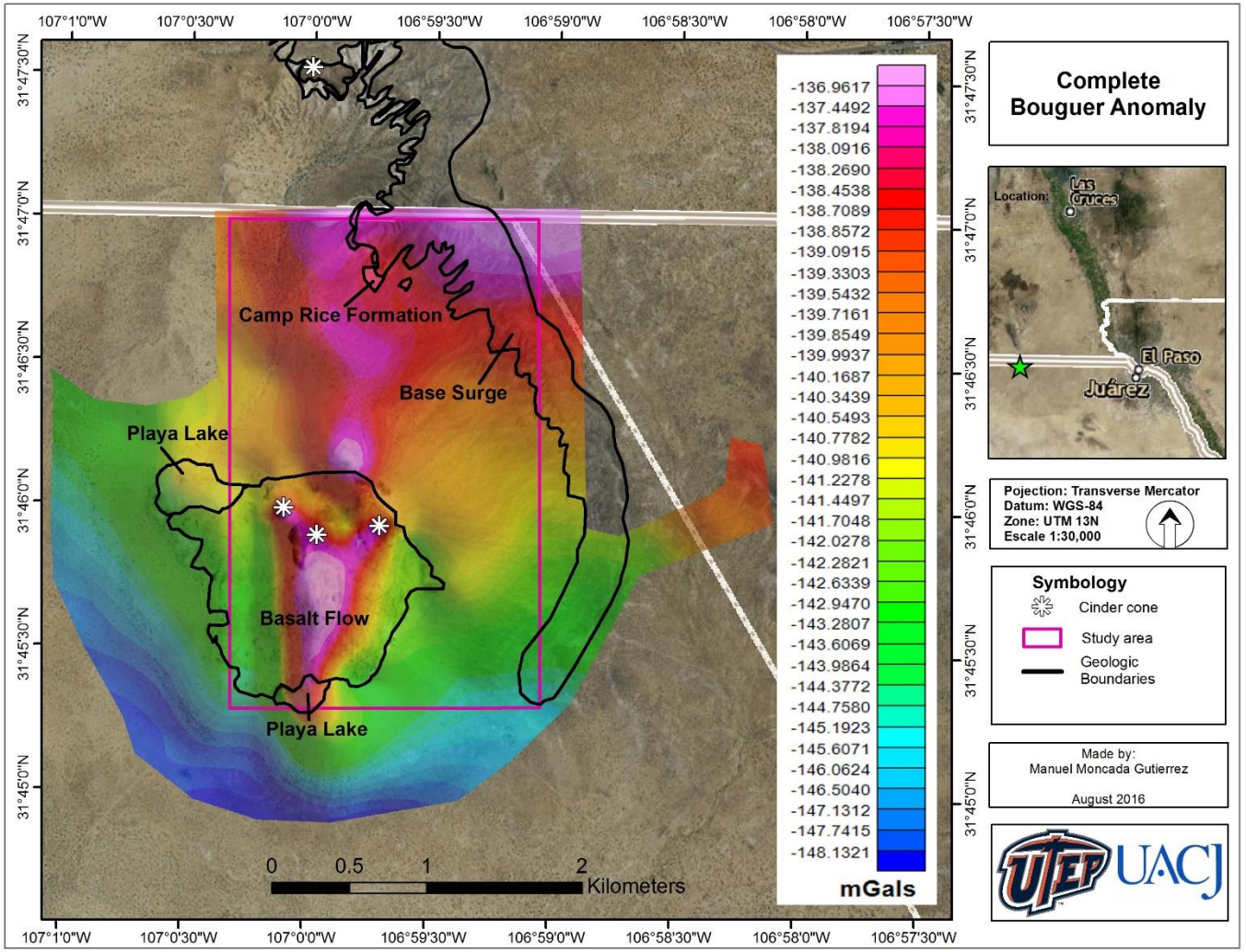

Figure 5.2 The CBA anomaly map for the study area. The main high anomalies (red to pink) values are related to main feeder located in the basalt flow at the surface. High anomalies in the northern part of the map are related to pre-maar lava flows from the scoria cone located in the U.S. part of Potrillo Maar.

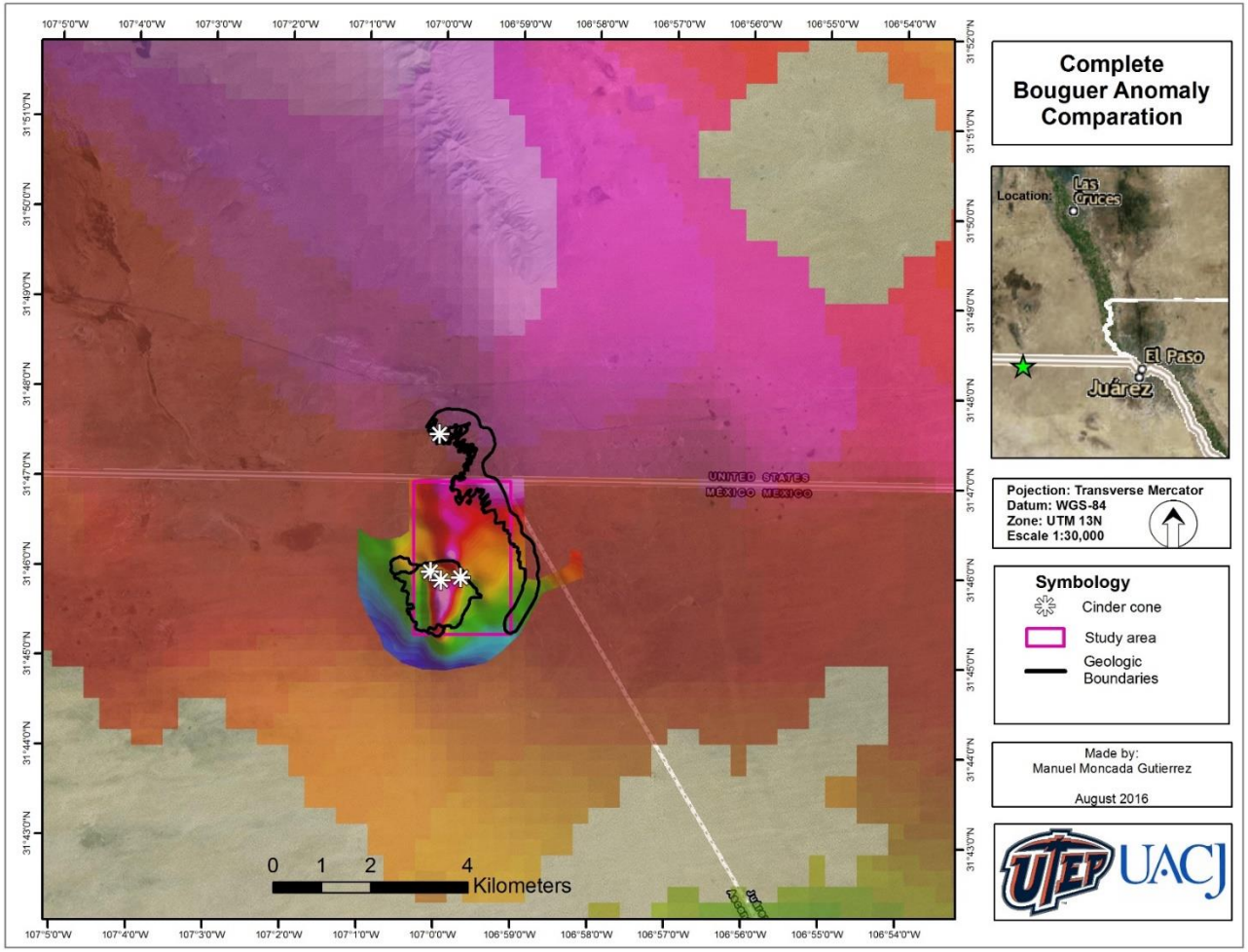

Figure 5.3 The regional CBA anomaly and local CBA anomaly in the study area. High anomaly values in the regional CBA anomaly are related to the deeper geological feature that controls the PVF. High values in the local CBA indicate the connection between Potrillo Maar and the PVF. It appears Potrillo Maar forms the southern end of the PVF gravity anomaly high.

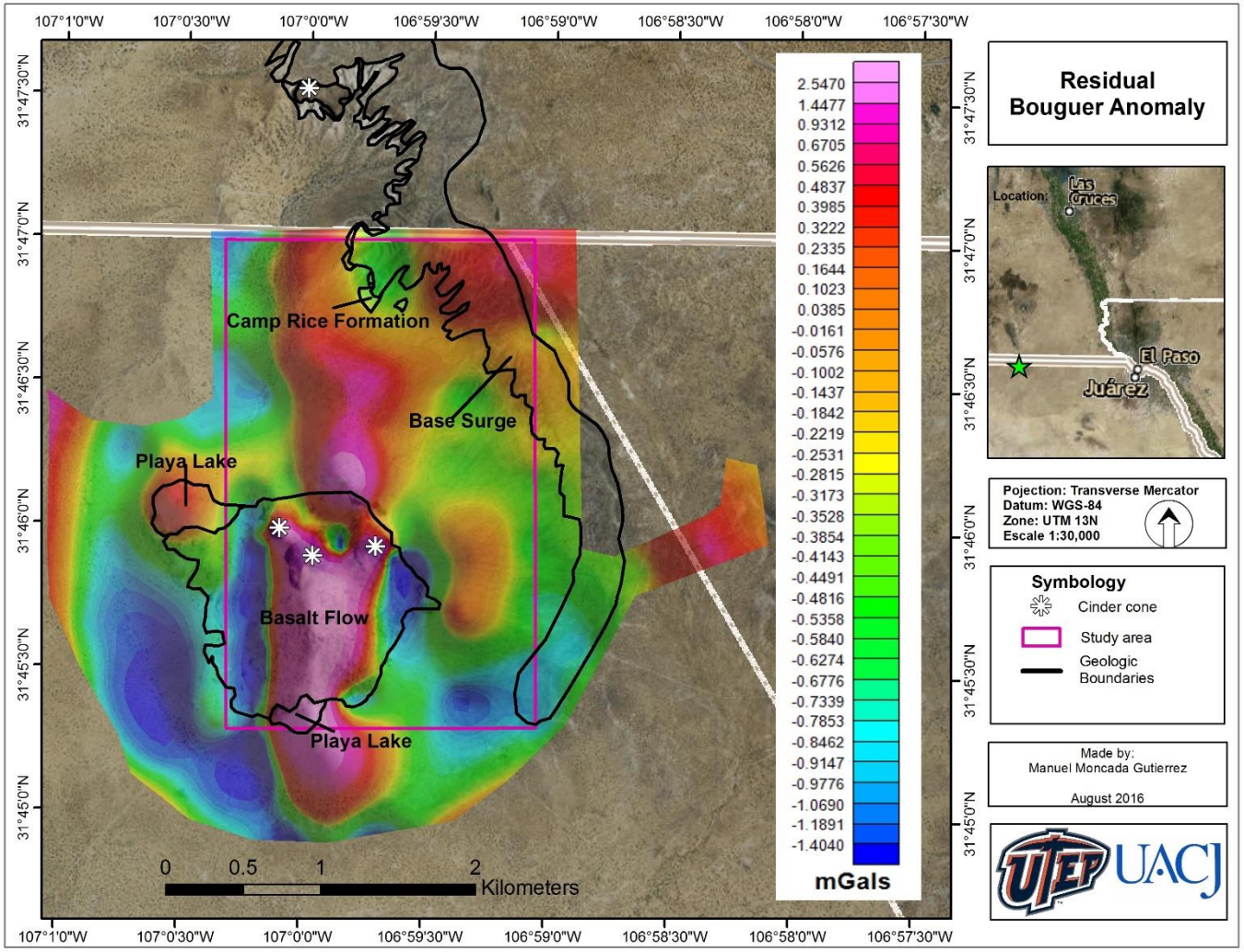

Figure 5.4 Residual Bouguer Anomaly map of the area of study. High anomaly values are related to basalt flows and structures that are exposed at surface (in the case of the high anomaly in the center of the map), or buried by sediments and pyroclastic ejecta (in the case of the anomalies located in the northern part of the map) and in the playa.

Magnetic maps

The RTP anomaly map (Figure 5.5) has a wide range of magnetic values ranging from 46800 nT to 48150 nT. The east and west scoria cones have relatively low magnetic values, while the scoria cone located at the center of the map has a high magnetic value. This difference can be related to the iron content of minerals present within the main feeder dike. A hand-hold susceptibility meter was used to compare variations in the susceptibility of surface deposits. Where the lava facies have a reddish color due to the iron oxide susceptibility values between 10 and $15x10^{-3}$ SI were measured, while the facies with lower iron content have a susceptibility between 2 to $10x10^{-3}$ SI. The highest RTP anomaly values located at the northern part of the scoria cones and in the southern part of the map are related to intrusive structures buried by superficial deposits.

The residual RTP map (Figure 5.6) was obtain by fitting a third-order polynomial to the longer wavelength regional trends to have just local features. The residual RTP shows the same high magnetic anomalies in the center of the map as well as low anomalies where the magnetic response ranges from -667.983 nT to 638.885 nT. Low values in the RTP are interpreted as the diatreme produced by the explosion that created the maar. The surface susceptibility survey at the surface was carried out to determine if negative susceptibility values were present in the lava flows, however, the data obtained from the surveys did not show any negative values. Also, age dating using $^{40}Ar/^{39}Ar$ in the center scoria cone by McIntosh (1994), reveal an age of 59,000 ± 10,000 years old. This means that the low magnetic anomalies need to be due to volcanic rocks that are older than 0.78 Ma, the last record of a geomagnetic reversal, that are not exposed at the surface. Pre-maar volcanism with an estimated of 700,000 years, could be the cause of these lows.

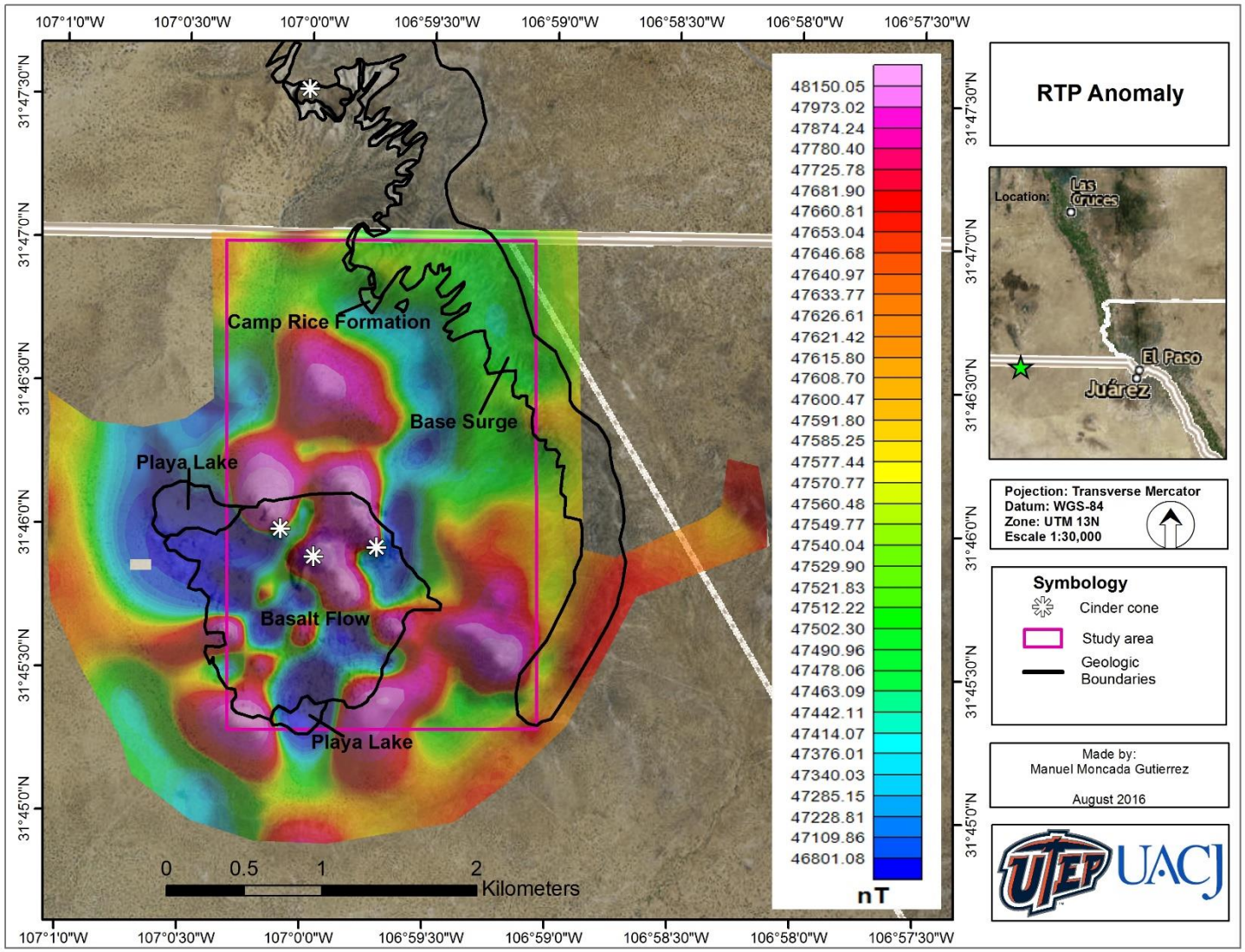

Figure 5.5 The Reduced To Pole anomaly values. High magnetic values are related to basaltic flows with high iron content. Low magnetic values are related to the diatreme of the maar.

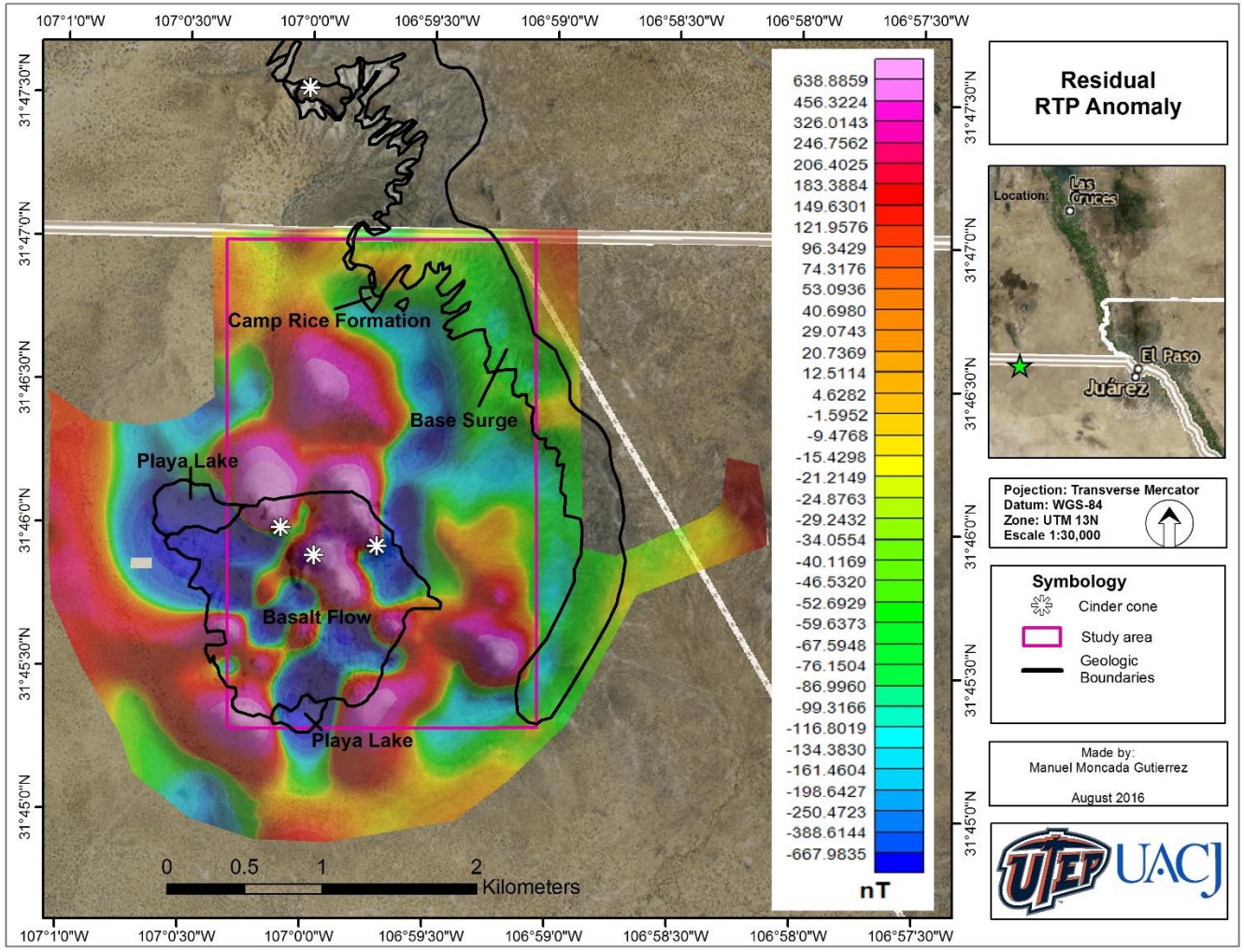

Figure 5.6 Residual RTP anomaly of the study area. The high magnetic anomalies represented by reddish colors are caused by basalts formation with high iron content. Negative magnetic readings (blue to yellow color) are interpreted as the part of the diatreme that is formed of pre-maar material (older than 0.78 Ma).

Electrical tomography

Line A-A'

This east-west oriented line is 800 meters long and sampled to approximately 225 meters in depth as shown in Figure 5.7. A wide range in resistivity is interpreted along this line from 3.81 to 167,093 Ωm with an error of 15.3 Ωm. The first 50 meters along the line (1225-1175 m) have a resistivity that goes from 7,883 to 167,093 Ωm and is attributed to the basalt flows at surface. This basalt is very vesicular making it very resistive due to the air in the pore space. The next 50 meters (1175-1125 m) have resistivity from 372 to 36,293 Ωm, these values can be cause by non-weathered basalt below the exposed lava flow. The main feature are the high resistivity values in the west and the lows in the east side of the line, clearly showing the division of the basalt and intrusions from the ejecta deposits.

Line B-B'

Tomography line B-B' has length of 1 kilometer and a penetration depth of 200 meters approximately (Figure 5.8). This line shows resistivity values that range from 3 Ωm to 31480492 Ωm with an error of 27.1 Ωm. The first 25 m depth are interpreted as a layer of sediments and weathered basalt flows. At 420 m along the tomography, the highest anomaly values in the whole line are observed, where the last 175 m depth is interpreted as a basaltic dike. Between 420 and 580 m, the tomography shows the lowest resistivity 175m depth. This anomaly is interpreted as the pyroclastic deposits from pre-maar and post maar volcanism due to the present of tuff that has low resistivity. An increment in resistivity in the last portion of the line is interpreted as part of a basaltic dike exposed at the surface at the end of the sounding.

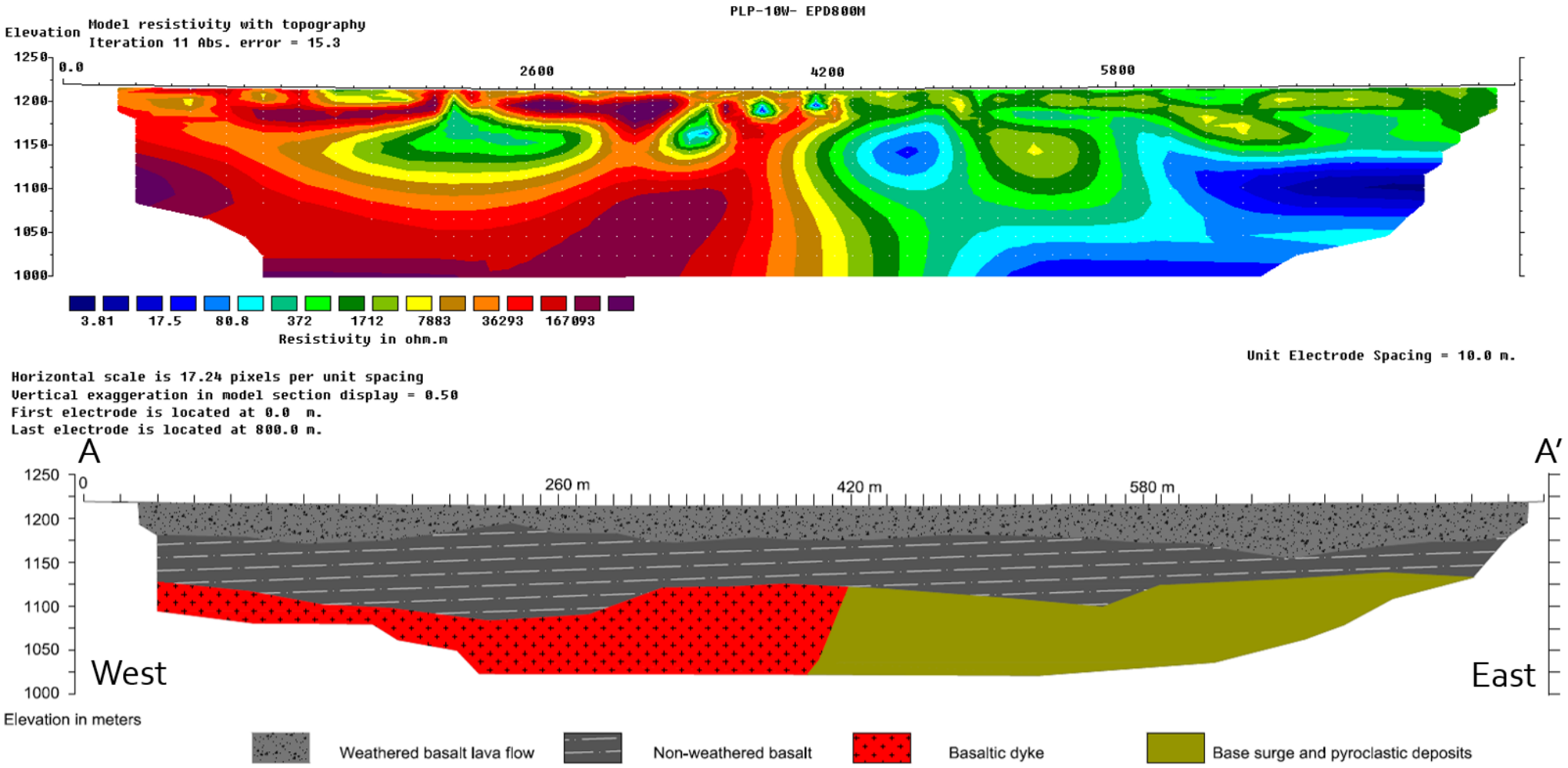

Figure 5.7 Result from inversion of the resistivity profile A-A' (top) and the interpreted structure (bottom).

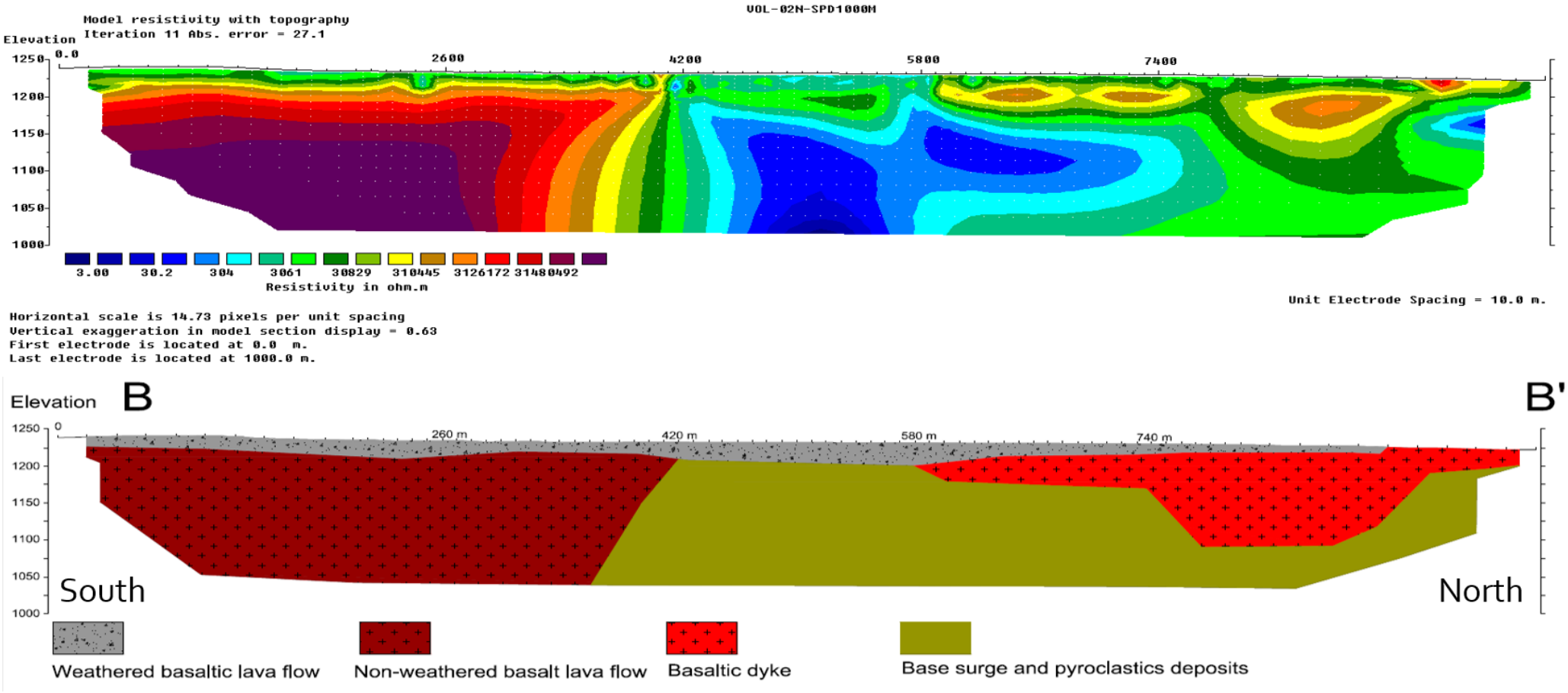

Figure 5.8 Result from inversion of the resistivity tomography B-B’ (top) and the interpreted structure (bottom).

Chapter 6 Data modeling

The final step in the investigation was the construction of two cross-sections across the maar volcano in order to accurately determine the geologic structures in the area. The location of the profiles is shown in figure 6.1. The Residual Bouguer Anomaly, Reduced To Pole magnetic anomaly and the electrical resistivity tomography were used to produce the models. The first transect (A-A') was located in the south part of the area of study with a west-east direction, where this profile crosses the tephra ring, base surge and ejecta deposits, and basalt lava flows. The second transect (B-B') was located in the central part of the study area and is oriented in a west–east direction, where this section crosses intersects the three scoria cones.

Gravity models were produced by forward modeling which consisted of creating a source body based on previous geological and geophysical studies of maar volcanoes. Then a density and magnetic inversion were conducted in order to determine a better approximation by reducing the error in the calculated and observed data. The final result was the model that better fits with the observed data but also a model that makes geological sense.

The densities and susceptibilities used for the construction of the models are based on previous studies of different maars. These densities values were used by Maksim (2016), Blaike et al (2012) and Skácelová et al (2010). Table 1 shows the density values of the geologic formations for the models.

Table 1. Densities and Susceptibilities of the rock units used for the constructed models.

Rock Unit	Magnetic Susceptibility (10^{-3} SI)	Density (kg/m^3)
Basaltic lava flows	0.032 to 0.048	2210 to 2348
Base surge and pyroclastic deposits	0.039 to 0.079	2124 to 2188
Diatreme	-0.249 to -0.193	2126 to 2823
Basaltic Feeder Dikes	0.05 to 0.17	2645 to 2686
Sediments	0	2000
limestone	0	2610

Interpretation of profile A-A'

Profile A-A' (Figure 6.2) is located in the southern part of the study area. Base surge and pyroclastic deposits cover the majority of the surface to 388 m depth. Those deposits corresponds to the smooth increments in the gravity and magnetic values and with the low resistivity values in the eastern part of the electrical tomography result (Figure 6.3). The two abrupt increments are related to the basaltic dike with an extension of 1,100 m approximately and with a depth extent of 70 m to 278 m. The shallower extension of the basaltic dike also has a good correlation with the electrical tomography in the western part of the profile. High resistivity values at the surface of the tomographic profile are related to basalt flows with a depth of 156 m that are exposed at surface. The diatreme body was located where the lowest values in the magnetic field occurrence. The high values in the magnetics and gravity appear to be associated with the basaltic dike. The magnetic data cannot be modeled unless a negative susceptibility body is used.

A density and magnetic values inversion were used to reduce the error between the observed and the calculated data by using values from previous works as constraints.

Mathematically it gave very good results by reducing the error along the profile but it does not match the geology well along A-A' because it gives by the diatreme that have a density of 4274 kg/m^3. This is too high for crustal materials in the Earth (Figure 6.4).

Interpretation of profile B-B'

The Profile B-B' (Figure 6.5) is located in the center part of the area of study trending a west-east direction and intersects the three scoria cones at the surface. Again, a base surge with pyroclastic deposits and basalt lava flows are present at surface with a modeled depths around 148m and 273 m for the base surge and 140 m to 156 m for the basalt flows. High magnetic and gravity values at the middle of the profile are located where there is a scoria cone. This cone is related to the main basaltic dike feeder that extends to the west and east of the profile. In profile A-A', this cross-section show low magnetic values and requires negative susceptibility values to model the observations and reduce the error. This suggest the diatreme is composed of pre-maar material of >0.7 Ma. In order to have negative values the diatreme has a depth of 125 m in the deepest part of the section. Part of the diatreme located in the center of the profile had to have positive susceptibility to match the profile. This could represents the result of mineralization, hydrothermal alteration, or partial melting to reset the polarity of magnetization.

An inversion was also run as in profile A-A' to reduce the error between the observed and calculated values. This inversion gave better results compared to the previous profile making reasonable between the mathematics and geology.

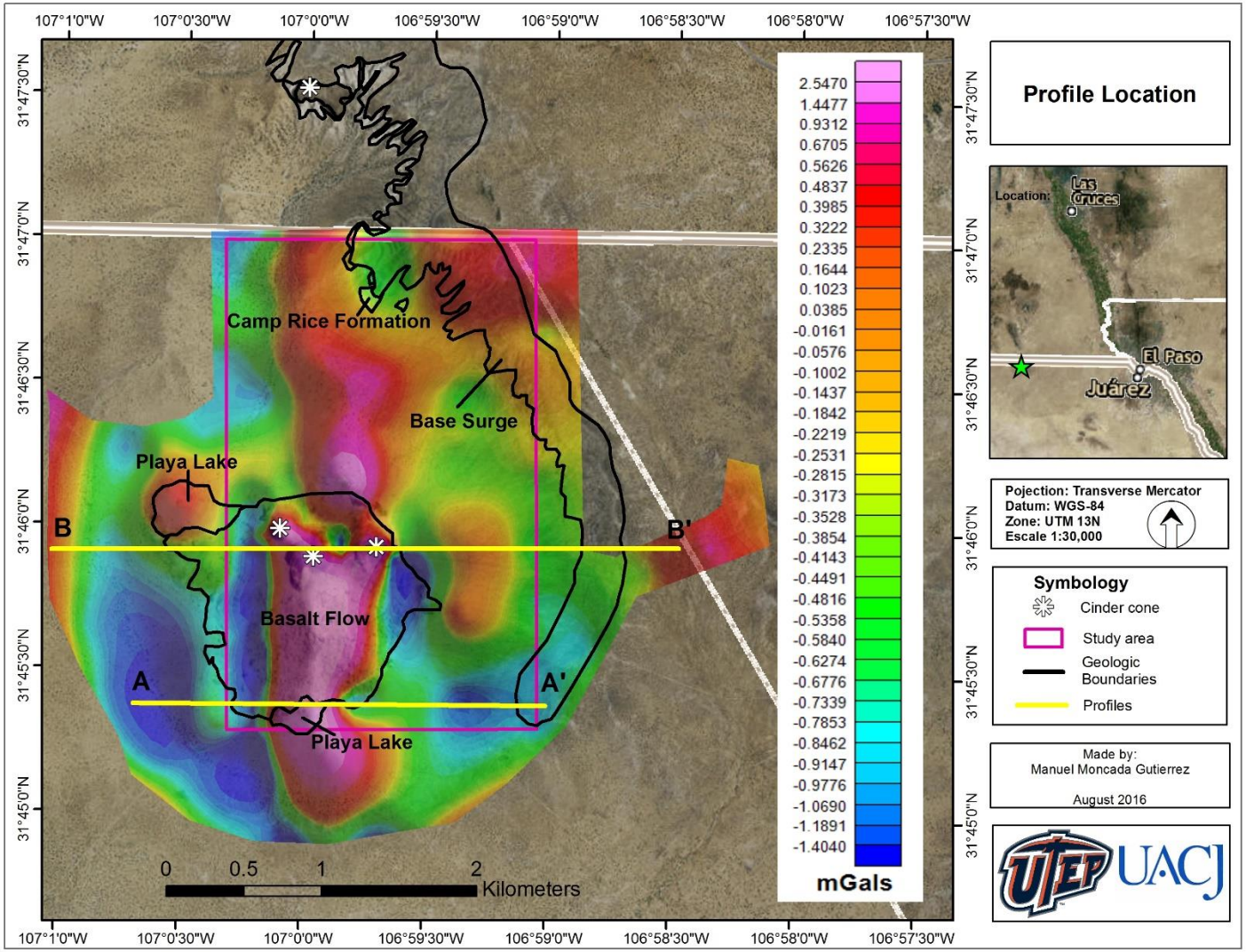

Figure 6.1 Location of showing modeled in the study area.

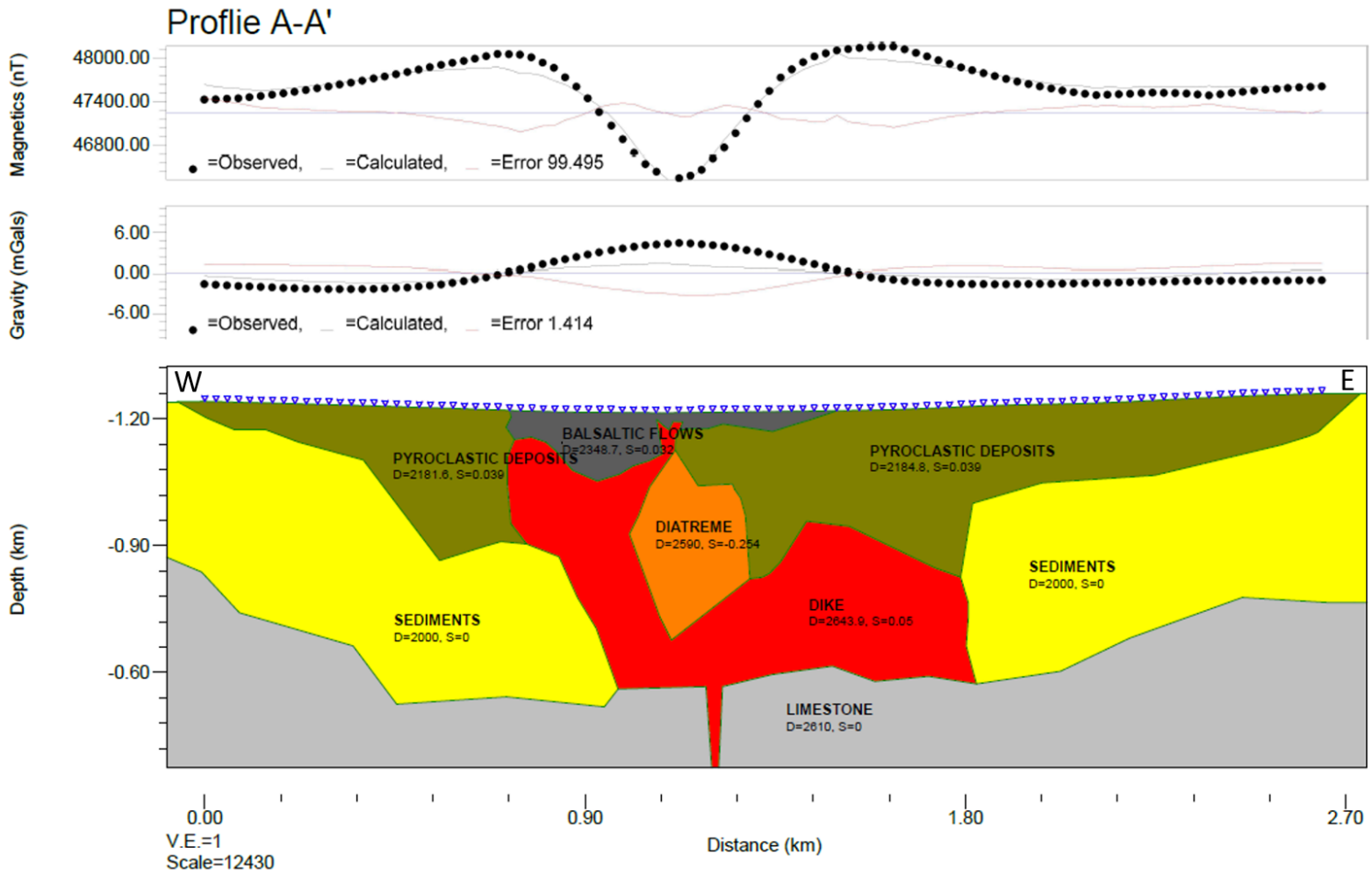

Figure 6.2. 2D model of profile A-A'. Density (D) in kg/m^3 and magnetic susceptibilities (S) in SI units are noted. It has an rms error of 1.414 mGals and 99.495 nT respectively.

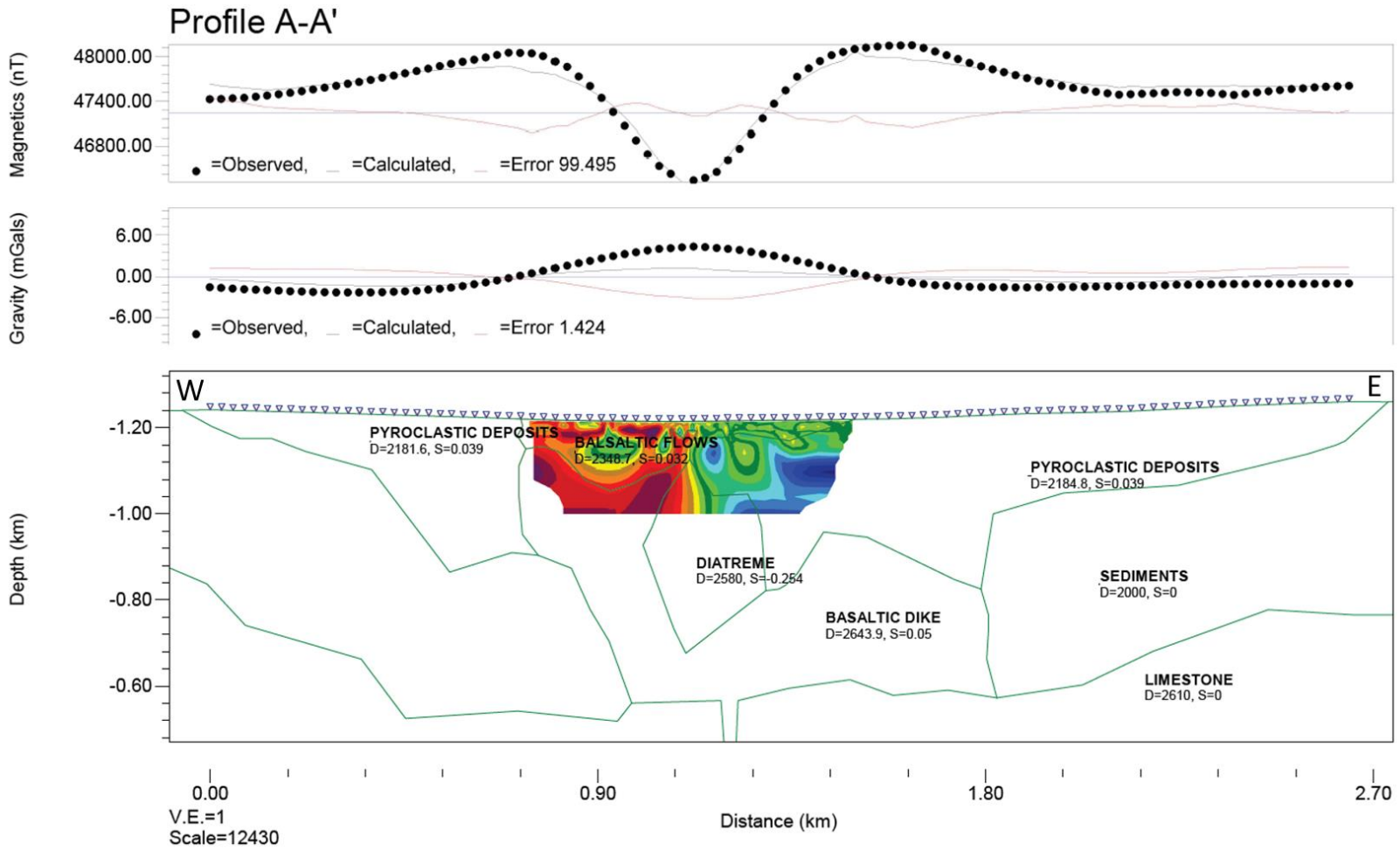

Figure 6.3 The model from profile A-A’ with the resistivity tomography overlay upon it. Note the good correlation of the tomography with the profile where the basaltic flows and dike, diatrem and pyroclastic deposits are well constrainted**.**

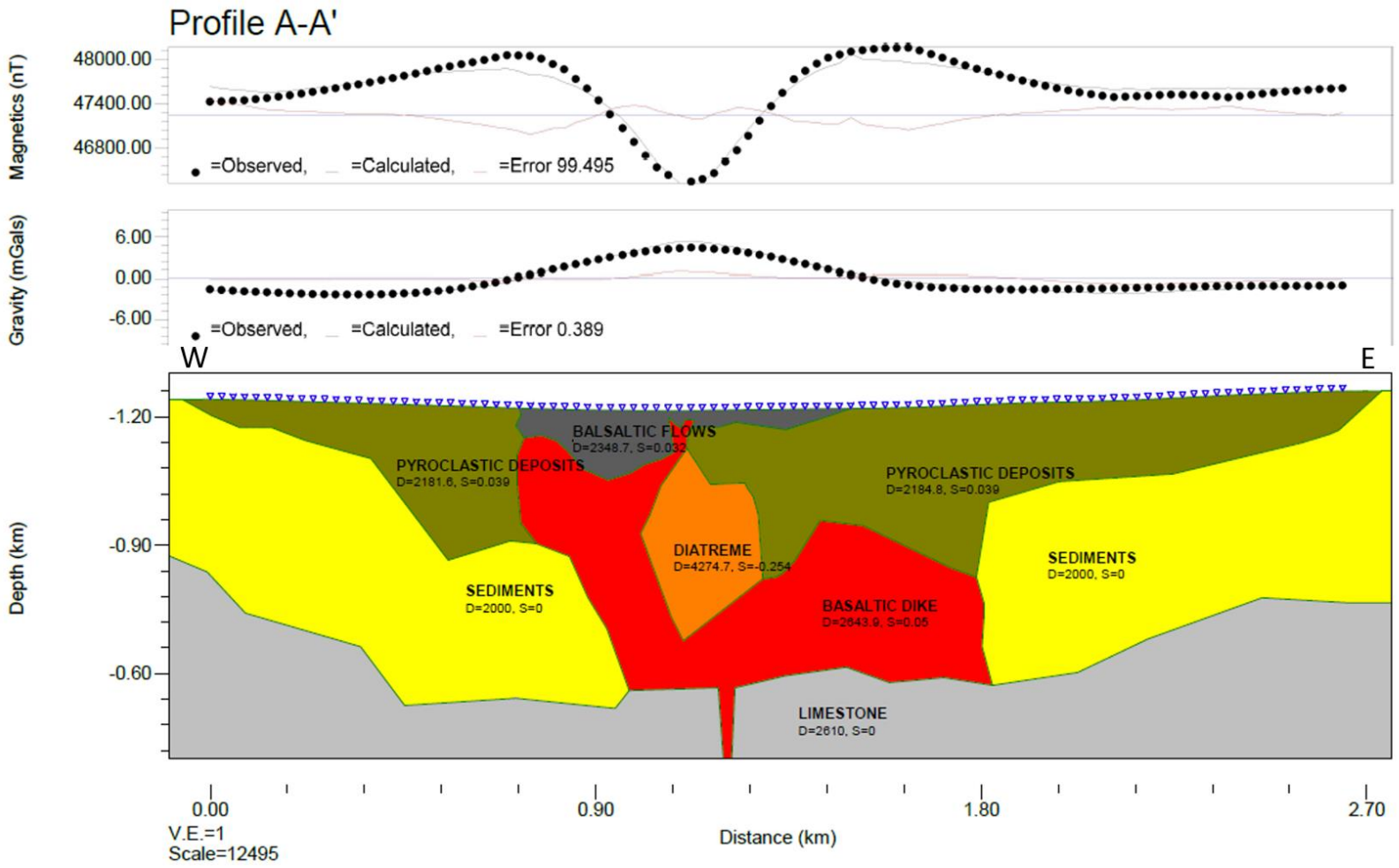

Figure 6.4 Profile A-A' with density and susceptibility values obtained from the inversion. The diatreme has an unacceptable density of 4247 kg/m^3.

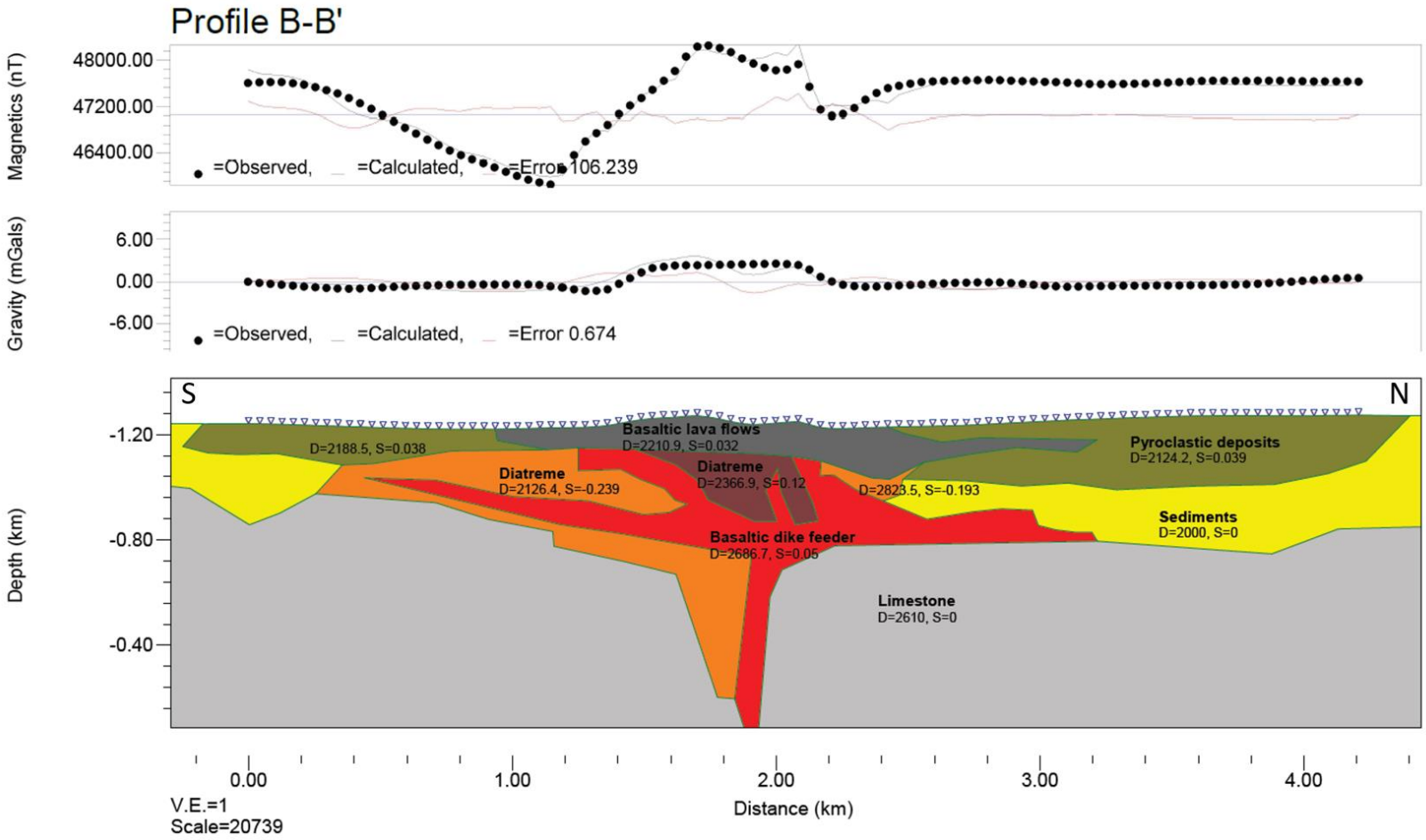

Figure 6.5 The 2D model for profile B-B'. This transect is located in the central part of the study area and intersects the scoria cones. It has an rms error of 106.239 nT and 0.674 mGals in the magnetic and gravity anomalies, respectevely.

Chapter 7 Conclusions

The Potrillo Maar of the Potrillo Volcanic Field shows complex structural features. Two dimensional modelling of the maar revealed information about the geometry of its underlying diatreme and feeder dikes that could not be detected by simply studying the maar geology at surface. Two diatreme structures were identified were the magnetic anomaly had negative values. Figure 7.1 shows a possible interpretation for the negative values based on Lorenz (2003). First the pre-maar eruptions occured, and deposit the pre-maar basaltic lava flow (>0.7 Ma) and base surge with pyroclastic deposits. After this, sediments were deposited and water may have been a conduit for infiltrated them. The Mount Riley fault zone activation of a new intrusion in the south part of Potrillo Maar. This new intrusion came in contact with the water table to produce steam and exploded due to the high pressures in the area and creates the maar-volcano with the tephra ring. Rock form the pre-maar and base surge material falls in the inverted cone produce by the explosion and by the pressure of overlaying layers it forms the diatreme. Magma rose through the pores of the diatreme until it reached the surface and the three scoria cones were formed.

Boreholes would be helpful to have better constraint two dimensional models by obtaining the susceptibility and density of the rocks at depth. In addition, it would be helpful to continue the geophysical surveys to the north within the U.S.

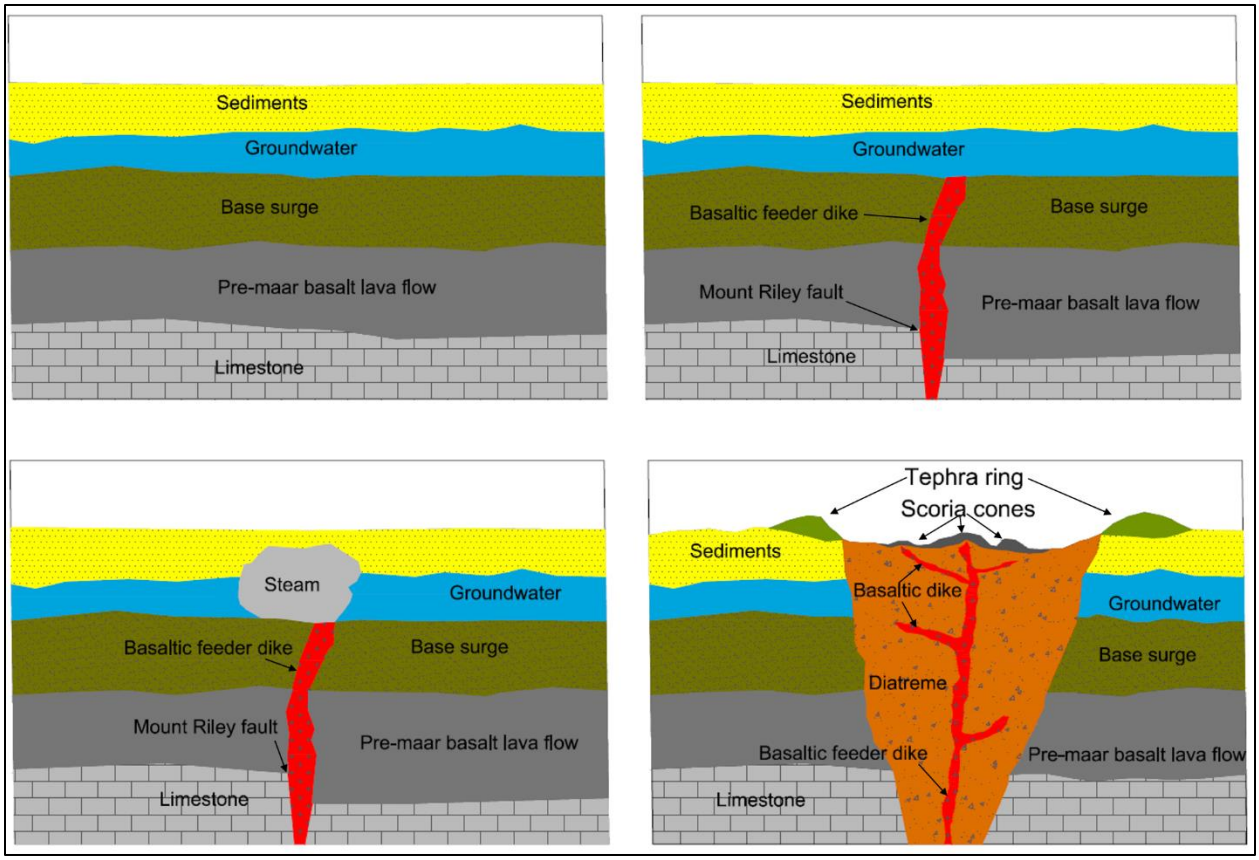

Figure 7.1 This figure shows the possible process Potrillo for formation of Maar.

Reference

Anthony, E.Y., Hoffer, J.M., Waggoner, W.K., Chen, W., 1992. Compositional diversity in late Cenozoic mafic lavas in the Rio Grande Rift and Basin and Range province southern New Mexico. Geological Society of American Bulletin v. 104, p. 973–979.

Bickford, M.E., Soegaard, K., Nielsen, K.C., and McLelland, J.M., 2000, Geology and geochronology of Grenville-age rocks in the Van Horn and Franklin Mountains area, west Texas: Implications for the tectonic evolution of Laurentia during the Grenville: Geological Society of America Bulletin, v. 112, p. 1134-1148.

Blaikie, T.N., Ailleres L., Cas, R.A.F., Betts, P.G., 2012. Three-dimensional field modelling of a multi-event maar-diatreme – The Lake Coragulac maar, Newer Volcanic Province, south-eastern Australia. Journal of Volcanology and Geothermal Research v. 235-236, p. 70-83.

Cassidy, J., France, S.J., Locke, C.A., 2006. Gravity and magnetic investigation of maar volcanoes, Auckland Volcanic Field, New Zealand. Journal of Volcanology and Geothermal Research v. 159, p. 153–163.

Cather, S.M., 2004, Laramide orogeny in central and northern New Mexico and southern Colorado: *In* Mack, G.H., and Giles, K.A., eds., The Geology of New Mexico: A Geologic History: New Mexico Geological Society Special Publication 11, p. 203-248.

Chapin, C.E., and Cather, S.M., 1981, Eocene tectonics and sedimentation in the Colorado Plateau–Rocky Mountain area: *In* Dickinson, W.R., and Payne, W.D., eds., Relations of Tectonics to Ore Deposits in the Southern Cordillera: Arizona Geological Society Digestv. 14 p. 173-198.

deGroot-Hedlin, C. and Constable, S., 1990. Occam's inversion to generate smooth, two dimensional models from magnetotelluric data. Geophysics, v. 55, p. 1613-1624.

Hamblock, J.M., 2006. Understanding the composition, origin, and evolution of the continental crust: case studies in the southern Rio Grande Rift, New Mexico, and the coast plutonic complex, British Columbia, Canada. Ph. D. Thesis,University of Texas at El Paso, Department of Geological Science, p. 226.

Hawley, J. W., 1975, Quaternary history of Dona Ana country region, south-central New Mexico, in Seager, W. R., Clemons, R. E., Callender, J. F. (eds.), New Mexico Geological Society 26th Annual Fall Field Conference Guidebook: New Mexico Geological Survey (Soccoro, NM), p. 68.

Hoffer, J. M., 1971, Mineralogy and petrology of the Santo Tomas-Black Mountain basalt field, Potrillo volcanics, south-central New Mexico: Geological Society of America Bulletin, vol. 82, no. 3, p. 603-612.

Hoffer, J.M., 2001. Geology of Potrillo Maar, southern New Mexico and northern Chihuahua, Mexico. New Mexico Museum of Natural History and Science Bulletin v. 18, p. 137–140.

Karlstrom, K.E., Amato, J.M., Williams, M.L., Heizler, M., Shaw, C.A., Read, A.S., Bauer, P., 2004. Proterozoic tectonic evolution of the New Mexico region: A synthesis. New Mexico Geology Society, The geology of New Mexico: A geologic history p. 1–34.

Li, Y., Barnes, M.A., Chattopadhyay, I., Barnes, C.G., Frost, C.D., 2004. U–Pb zircon ages of surface and subsurface samples from Texas and Southern New Mexico: implications for Grenville-age and Tertiary magmatism. Geological Society of America Abstracts with Programs 36 (5), p. 147.

Lorenz V., 2003. Maar–diatreme-volcanoes, their formation and their setting in hard-rock or soft-rock environments. Geolines, v. 15, p. 72–83.

Mack, G.H., 2002. Middle and late Cenozoic crustal extension, sedimentation, and volcanism in the southern Rio Grande rift, Basin and Range, and southern transition zone of southwestern New Mexico. The geology of New Mexico: A geologic history 11, p. 389–406.

Maksim, N. 2016. An integrated geophysical survey of Killbourne Hole, southern New Mexico: Implications for near surface exploration of maars and the Moon.

McIntosh, W.C., 1994. $^{40}Ar/^{39}Ar$ Geochronology of Late Miocene to Pleistocene basalts of the Zuni Bandera, Red Hill-Quemado and Potrillo Volcanic Fields, New Mexico Geology, v. 16, p. 60-61.

McMillan, N.J., Dickin, A.P., and Haag, D., 2000, Evolution of magma source regions in the Rio Grande Rift, southern New Mexico: Geological Society of America Bulletin, v. 112, p. 1582-1593.

Reiche, P., 1940, The origin of Kilbourne Hole, New Mexico: American Journal of Science, vol. 238, no. 3, p. 212-225.

Rapid 2-D Resistivity & IP inversion using the least-squares method Wenner (α, β, γ), dipole-dipole, inline pole-pole, pole-dipole, equatorial dipole-dipole, offset pole-dipole, Wenner-Schlumberger, gradient and non-conventional arrays On land, water and cross-borehole surveys. Geotomo Software, Penang, Malaysia, 2010.

Sasaki, Y. 1992. Resolution of resistivity tomography inferred from numerical simulation. Geophysical Prospecting, v. 40, p. 453-464.

Seager, W. R., 1987, Caldera-like collapse at Kilbourne Hole maar, New Mexico: New Mexico Geology Science and Service, vol. 9, no. 4, p. 69-73.

Seager, W.R., 2004, Laramide (Late Cretaceous–Eocene) tectonics of southwestern New Mexico: *In* Mack, G.H., and Giles, K.A., eds., The Geology of New Mexico: A Geologic History: New Mexico Geological Society Special Publication 11, p. 183-202

Shannon, W.M., Barnes, C.G., Bickford, M.E., 1997. Grenville magmatism in West Texas: petrology and geochemistry of the Red Bluff granitic suite. Journal of Petrology 38, p. 1279–1305.

Skácelová, Z., Rapprich, V., Valenta, J., Hartvich, F., Šrámek, J., Radon, M., Gazdová, R., Nováková, L., Kolínsky, P., Pécskay, Z., 2010. Geophysical research on structure of partly eroded maar

volcanoes: Miocene Hnojnice and Oligocene Rychnov volcanoes (northern Czech Republic). Journal of Geoscience v. 55, p. 333–345.

Talwani, M.,Worzel, J.L., Landisman, M., 1959. Rapid gravity computations for two dimensional bodies with applications to the Mendocino Submarine Fracture Zone. Journal of Geophysics, v. 64, p. 49-59.

Talwani, M., Heirtzler, J.R., 1964. Computation of magnetic anomalies caused by two-dimensional structures of arbitrary shape, computers in the mineral industries: School of Earth Sciences, Stanford University (Publication), p. 464-480.

Waggoner, W. K., 1990, Petrology and geochemistry of mantle-derived lavas from Potrillo Maar, New Mexico and Chihuahua, Mexico. M.S. Thesis, University of Texas at El Paso, p. 69.

White, J.D.L., Ross, P.-S., 2011. Maar-diatreme volcanoes: A review. Journal of Volcanology and Geothermal Research, from maars to scoria cones: the enigma of monogenetic volcanic fields, p. 11.

Williams, W.J.W., 1999, Evolution of Quaternary intraplate mafic lavas detailed using 3He surface exposure and 40Ar/39Ar dating, and elemental and He, Sr, Nd, and Pb isotopic signatures: Potrillo Volcanic Field, New Mexico, U.S.A., and San Quintin Volcanic Field, Baja California Norte, Mexico [Ph.D. thesis], University of Texas at El Paso, 195 p.

Curriculum Vita

Manuel Moncada Gutierrez was born in Ciudad Juarez, Chihuahua, Mexico. The third child of Manuel Moncada Marrufo and Olga Gutierrez Contreras. He obtained a Bachelors degree of in Physics from Universidad Autonoma de Ciudad Juarez (UACJ) in 2011. During his career, he worked in the Centro de Informacion Geografica in UACJ and had three internships with the mining company Peñoles. Later, he was accepted into the Geophysics graduate program in 2014 at University of Texas at El Paso (UTEP) were obtained his MS in geophysics in December 2016.

Contact Information: mmoncada.gutierrez@gmail.com

Permanent address: Fierro 136 Sur. Gregorio M. Solis
Ciudad Juarez, Chihuahua, Mexico
CP 32160

This thesis was type by:
Manuel Moncada Gutierrez